Establishment and Characterization of a Unilateral UV-Induced Photoreceptor Degeneration Model in the C57Bl/6J Mouse

Anna-Marina van der Meer[1], Tanja Berger[2], Frank Müller[3], Ann Christina Foldenauer[2,4], Sandra Johnen[1], and Peter Walter[1]

[1]Department of Ophthalmology, University Hospital RWTH Aachen, Pauwelsstr. 30, 52074 Aachen, Germany

[2]Department of Medical Statistics, RWTH Aachen University, Pauwelsstr. 19, 52074 Aachen, Germany

[3]Institute of Complex Systems, Cellular Biophysics, ICS-4, Forschungszentrum Jülich GmbH, 52428 Jülich, Germany

[4]Department of Clinical Research Fraunhofer Institute for Molecular Biology and Applied Ecology (IME) Branch for Translational Medicine and Pharmacology (TMP), Theodor-Stern-Kai 7, 60590 Frankfurt, Germany

corresponding author: Univ.-Prof. Dr. med. Peter Walter, pwalter@ukaachen.de, Department of Ophthalmology, University Hospital RWTH Aachen, Pauwelsstr. 30, 52074 Aachen, Germany

All authors revised the paper.

No. of pages: 63

No. of figures: 14

No. of tables: 9

No. of words Abstract: 250/250

Conflict of Interest: The authors declare no commercial relationship (N).

This work was supported by the Deutsche Forschungsgemeinschaft (www.dfg.de) (grants WA1472/6-3, JO1263/1-3, MU3036/3-3).

Abstract

Purpose: To investigate, whether UV irradiation of the mouse eye can induce photoreceptor degeneration, producing a phenotype reminiscent of the rd10 mouse, left eyes of female C57Bl/6J mice were irradiated with a UV LED array (370 nm). A lens was placed between cornea and LED, allowing illumination of about one third of the retina. The short-term and long-term effects on the retina were evaluated.

Methods: First, a dose escalation study, in which corneal dosages between 2.8 and 9.3 J/cm^2 were tested, was performed. A dosage of 7.5 J/cm^2 was chosen for the following characterization study. Before and after irradiation slit-lamp examinations, full-field electroretinography (ffERG), spectral domain optical coherence tomography (sd-OCT) and macroscopy were performed. After different time spans (5 days to 12 weeks) the animals were sacrificed and the retinae used for immunohistochemistry or multielectrode array (MEA) testing. Right eyes served as untreated controls.

Results: In treated eyes, sd-OCT revealed a decrease in retinal thickness to 53 %. ffERG responses decreased significantly from day five on in treated eyes. MEA recordings revealed oscillatory potentials with a mean frequency of 5.2 $\pm$ 0.6 Hz in the illuminated area. Structural changes in the retina were observed in immunohistochemical staining.

Conclusion: UV irradiation proved to be efficient in inducing photoreceptor degeneration in the mouse retina, while leaving the other retinal layers largely intact. The irradiated area of treated eyes can be identified easily in sd-OCT and in explanted retinae.

Translational Relevance: This study provides information on anatomical and functional changes in UV-treated retina, enabling the use of this model for RP-like diseases in animals suited for experimental retinal surgery.

Introduction

Retinal degenerative diseases, like retinitis pigmentosa (RP), impact the quality of life in affected patients and their relatives [1, 2, 3]. Helping these patients preserve or regain vision is important. Electrical stimulation with retinal prostheses is one solution to tackle vision loss [4, 5, 6, 7, 8, 9, 10, 11]. The technology has reached clinical application and patients have successfully been implanted with different devices [12, 13, 14, 15, 16, 17, 18].

During the progression of RP, photoreceptors (PRs) degenerate while the inner retina is largely unharmed [8]. Due to the loss of afferentiation from PRs, the layers of the inner retina undergo a process known as *remodeling* [19]. Since the retinal ganglion cells remain intact, they are a frequent target of electrical stimulation by prostheses. By electrically stimulating ganglion cells, phosphenes can be elicited, enabling the restoration of some residual vision [20].

To improve such retinal prostheses, large-eye animal models are needed. Aside from the well described retinal degeneration 1 (rd1) and retinal degeneration 10 (rd10) mouse and Royal College of Surgeons (RCS) rat – genetic models for RP – few genetic models exist in larger species like dog [21], cat [22], rabbit [23] or miniature pig [24]. Disadvantages of genetic large-species models are the slow disease progression and the lack of an intraindividual control eye. Both can be avoided by inducing PR degeneration experimentally in only one eye.

The harmful effect of light on the eye has been investigated as early as 1889 [25] and the effect on the retina in more detail since the 1960's [26]. Today, it is known that light exposure can damage PRs via non-thermal mechanisms. The effect on the retina depends on duration and intensity of light exposure, wavelength, state of dark adaptation, retinal location, age, previous light exposure as well as characteristics and distribution of light absorbing chromophores [27, 28].

The fact that the retina of the rhesus monkey is most susceptible to damage by light in the UV range, was found by Ham et al. in 1979 [29]. This was confirmed in experiments with aphakic rhesus monkeys, where the retinae were six times more sensitive to light with 350 and 325 nm wavelength, than to blue light with 441 nm [30]. Van Norren et al. published similar findings obtained from rat retinae in 1990 [31]. For the establishment of a PR degeneration model with an intact inner retina, it is important to know which cells are targeted by different wavelengths. In the squirrel retina, exposure to 366 nm at threshold intensity affected PRs only, whereas irradiation with 441 nm affected both, retinal pigment epithelium (RPE) and PRs [32]. Gorgels et al. published related findings in pigmented Long Evans rats: in the range of 320-440 nm, PRs suffered the most severe damage, whereas the RPE was targeted at 470-550 nm [33].

According to Henriksson et al., the C57BL/6 mouse cornea transmits approx. 50 % and the lens 55 % of the radiation at 370 nm (approximated from figure 3 and 4, [34]), which are important information for calculating the retinal irradiance.

A very useful compilation of research done on light induced retinal damage was put together by van Norren and Gorgels in 2011 [28]. Extensive research on light-induced damage to the retina was also conducted by Grimm and Remè [35, 36, 37, 38].

Here, we report the short and long term effects UV radiation had on the mouse retina and compare the produced phenotype to that of the rd10 mouse and the mouse model of n-nitroso-n-methylurea (MNU)-induced PR degeneration, before attempting to transfer the method to the large-eye rabbit model. The goal is to generate a model that is characterized by PR degeneration and

an intact ganglion cell layer, making it suitable for establishing surgical procedures for retinal prostheses and experiments on bridging the gap between light detection and signal transmission to the brain.

Material and Methods

All experiments were performed in accordance with the "ARVO Statement for the Use of Animals in Ophthalmic and Vision Research", the "German Animal Welfare Act" and after approval was obtained by the regulatory authorities (84-02.04.2011.A386 and 84-02.04.2017.A202). All efforts were made to minimize the number of experimental animals and their suffering. Animal numbers for this study were calculated by the Department of Medical Statistics.

Experimental Design and Statistical Analysis

The experimental design was reviewed at the Department of Medical Statistics (Chair: Univ.-Prof. Dr. rer. nat. Ralf-Dieter Hilgers). For the comparison of spectral domain optical coherence tomography (sd-OCT) and full-field electroretinography (ffERG) between the treated and the untreated eye, a linear mixed effects model with point in time, eye, baseline (0d) and interaction between point in time and eye as fixed effects and animals as random effect was fitted to the data, using unstructured as covariance structure. Test results were considered statistically significant when $p < 0.05$, while we adjusted for multiplicity with Holm-Scheffe procedure. Post hoc tests compared the treated and untreated eyes for fixed points in time and the points in time among each other separately for both eyes. All other outcomes were analyzed using two-sample or one-sample Student's t-test. All statistical analyses were performed using SAS V9.4 Software (SAS Institute Inc., Cary, NC, USA) and GraphPad Prism 6 (GraphPad Software Inc., La Jolla, CA, USA).

In the dose escalation study, a suitable dosage of UV radiation was sought. Therefore, dosages between 2.8 J/cm² and 9.3 J/cm² were tested. Eight animals were tested with 2.8, 3.7, 5.6, 6.5, 6.5, 9.0, 9.3, 9.3 J/cm², respectively. Please note that dosages are always given as measured on corneal surface, not on retinal surface, if not explicitly stated otherwise.

For the calculation of retinal dosages, the following formula (from [28] was used:

$$E_{ret} = E_{cor} \cdot \frac{\pi D^2}{4} \cdot \frac{\tau}{A_{ret}}$$

Corneal irradiance (E_{cor}) can be converted into retinal irradiance (E_{ret}) with D as pupil diameter (= 1.9 mm; from [39]), A_{ret} as irradiated retinal area (= 4.0 mm²; from Figure 2 C) and τ as the transmittance of the ocular media (= 0.35; from [34]). For example, a corneal irradiance of 7.5 J/cm² in our case equals a retinal irradiance of 1.87 J/cm².

For further dosage calculation refer to Supplementary Material - Dosage Calculation.

In the dose escalation study, pre-examinations (slit lamp examination, sd-OCT, ffERG, macroscopic images) were performed. One week later, the left eye was irradiated with the respective dosage and one, two and three weeks after the irradiation, follow-up examinations (macroscopic images, ffERG, sd-OCT) were performed. Three weeks after irradiation, the animals were sacrificed and the eyes prepared for H&E staining.

The characterization study involved four experimental groups – all groups received a pre-examination one week before irradiation (0d), involving macroscopy, ffERG and sd-OCT. Follow-up examinations included macroscopy, ffERG and sd-OCT as well. The groups differed in total follow-up time span (5 days, 6

weeks, 8 weeks, 12 weeks) after irradiation with 7.5 J/cm^2. Within the short term group, animals were examined five days (5d) after irradiation and single animals (n = 1) received follow-up examinations at one day (1d), two days (2d) and four days (4d), respectively. These single animals served to find the point in time, where half of the PRs were gone. For 1d, 2d and 4d after irradiation only exemplary data are shown, since statistical evaluation was not possible. A middle term group received follow-up examinations at one, two, four and six weeks (1w, 2w, 4w, 6w), and two long term groups received follow-up examinations at eight as well as at eight and twelve weeks (8w, 12w) after irradiation, respectively. All animals were sacrificed in the end. The eyes of one half of each group (n=4) were prepared for multielectrode array (MEA) recordings, the other half (n=4) for immunohistochemical stainings.

Animals

Female C57Bl/6J mice (aged 7-11 weeks, average age 8.8 $\pm$ 0.9 weeks; RRID: IMSR_JAX:000664) were housed under controlled cyclic environmental conditions (Charles River Laboratories GmbH & Co. KG, Sulzfeld, Germany: 16:8 hr light/dark cycle, $<$ 60 lux inside the cages; animal housing facility of the Institute of Laboratory Animal Science, University Hospital RWTH Aachen, Aachen, Germany: 12:12 hr light/dark cycle, $<$ 100 lux inside the cages) with food and water available *ad libitum*. All animals were obtained from Charles River Laboratories GmbH & Co. KG, Sulzfeld, Germany ("https://www.criver.com/products-services/find-model/jax-c57bl6j-mice?region=23").

Anesthesia

For all experimental procedures (UV irradiation, sd-OCT, ffERG) the animals were anesthetized with an intraperitoneal injection of a mixture of xylazine (10 mg/kg Xylazin 2 % Bernburg®, Medistar, Ascheberg, Germany) and ketamine (60 mg/kg Ketamin® 10 %, CEVA, Düsseldorf, Germany), 1:10 diluted in saline. For longer anesthesia periods, 0.05 ml of the ketamine-xylazine mixture were applied subcutaneously in the lumbar region every 20 minutes. The animals were kept on a heated plate at 37 °C during anesthesia to maintain body temperature. When the animals were euthanized at the end of the experiment, they were decapitated in deep ketamine/xylazine anesthesia.

Ray Tracing Simulation

The ray tracing simulation was performed at the Chair for Technology of Optical Systems (TOS; Chair: Prof. Dr. rer. nat. Loosen), using "Zemax Optic Studio" (15.5 SP2, ZEMAX LLC., Kirkland, WA, USA). The Light-Emitting Diode (LED) we used for our experiments (370 nm LED Area Light, ProPhotonix Ltd., Salem, NH, USA) was characterized for its power at 1 cm, 5 cm and 10 cm distance, using a UV sensor (UV-sensor SI1 for UV LED 395 nm, 20 mW/cm² + Handheld HI1 for UV sensors, UV-Technik Meyer GmbH, Ortenberg, Germany). Data on the optical properties of the mouse eye, collected from different sources were provided, to determine the beam path within the eye [39, 40, 41]. A standard plano-convex lens (LA1274-A-N-BK7 Plano-Convex Lens, ⌀ = 30.0 mm, f = 40.0 mm, AR Coating: 350-700 nm; Thorlabs Inc., Newton, NJ, USA) was inserted in the simulated beam path at different distances and the illuminated retinal area was evaluated for size and homogeneity. The LED array was equipped with a heat sink (LED Area and Spot Light Heat Sink, ProPhotonix Ltd.) and a current controller (DC current controller, 0.75 A, 24 V

output, StockerYale Inc., Salem, NH, USA; operated at 0.4 A) and was additionally cooled with a standard table fan.

UV Irradiation

Before each irradiation, the UV light (AF1-370-IXF-100, Edmund Optics GmbH, Mainz, Germany; peak emission 370 nm ± 9 nm) was tested with a UV sensor (UV-sensor SI1 for UV LED 395 nm, 20 mW/cm² + Handheld HI1 for UV sensors, UV-Technik Meyer GmbH, Ortenberg, Germany) for correct intensity and possible heat generation (Checktemp® I Digital Thermometer - HI98509, Hanna Instruments Deutschland GmbH, Vöhringen, Germany). For the UV irradiation of the left eye, the anesthetized mouse was repeatedly treated with mydriatic eye drops (phenylephrin 2.5 g in 10 ml, tropicamide 0.5 g in 10 ml, prepared by the pharmacy of the University Hospital Aachen, Aachen, Germany), as well as with local anesthetics (Proxymetacaine hydrochloride eye drops 0.5 %; Proparakain-POS®, Ursapharm, Saarbrücken, Germany). The right control eye was treated with Bepanthen® eye ointment (5 % dexpanthenol, Bayer Leverkusen, Leverkusen, Germany) to prevent irritation and to block scattered UV light. The control eye was always turned in the opposite direction of the light source and was additionally covered by tissues. The mouse was then placed on a foam bed on a heating plate and the distance and alignment were adjusted: distance from LED housing to lens = 1 mm; distance from lens to cornea = 1 cm. During the dose escalation study, the eyes were irradiated with 2.8 - 9.3 J/cm² and regularly moisturized with saline during the irradiation. After irradiation, macroscopic images of both eyes were taken. To avert pain, animals were given a subcutaneous injection of 5 mg/kg Rimadyl® (carprofen 50 mg/mL, Pfizer Deutschland GmbH, Orth a.d Donau, Germany), 1:50 diluted in physiological saline. After irradiation and the following three days, the irradiated left eyes

were treated with antiphlogistic eye ointment (Isopto-MAX®, Alcon Pharma GmbH, Freiburg Breisgau, Germany) twice a day. During the characterization study, the eye was irradiated 8 minutes and 17 seconds, corresponding to 7.5 J/cm^2 on the corneal surface. The eye was kept moist by application of Methocel® 2 % (methylcellulose, Omnivision, Puchheim, Germany) every two minutes. Other than that, the protocol from the dose escalation study was followed. Irradiation was always performed between 2 and 4 p.m. after one hour of dark adaptation.

Spectral domain Optical Coherence Tomography

Sd-OCT scans were performed using the Spectralis® OCT system (Heidelberg Engineering GmbH, Heidelberg, Germany) according to the protocol by Rösch et al. [42]. The infrared (InRe) image (wavelength 715 nm) of the fundus was used for localization and size estimation of the degenerated retinal area. The optic nerve head was visible in all InRe images and served as a landmark. For thickness measurements of the retina, a crosshairs was centered on the optic nerve head and thickness measurements were performed in five fixed positions (see Figure 1; Heidelberg Eye Explorer V. 1.9.13.0, 2016 Heidelberg Engineering GmbH). In order to evaluate whether the inner retina was affected by the UV irradiation, thickness measurements of the inner retina were analyzed. Inner retina measurements were performed from ganglion cell layer to outer plexiform layer in the exact same positions as measurements of the overall retinal thickness. In treated eyes, the thickness was measured exclusively in the irradiated area. Averages from the five positions were calculated and the mean values analyzed with a linear mixed effects model with point in time, eye, baseline (0d) and interaction between point in time and eye as fixed effects and animals as random effect was fitted to the data, using unstructured as covariance structure.

Test results were considered statistically significant when $p < 0.05$, while we adjusted for multiplicity with Holm-Scheffe procedure. Post-hoc tests compared the treated and untreated eyes for fixed points in time and the points in time among each other separately for both eyes.

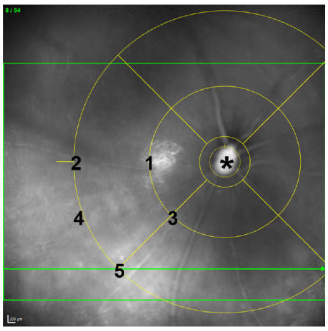

Figure 1: Positions of sd-OCT thickness measurements.
InRe image of a mouse fundus. Yellow: crosshairs for fixed thickness measurement positions (1-5). Green line intersecting number 5 is the position of the cross-sectional (CS) image in D. * = optic nerve head.

Electroretinography

ffERG recordings were performed using the Roland Consult recording System (Roland Consult Stasche & Finger GmbH, Brandenburg a.d. Havel, Germany) as described by Rösch et al. [42]. The animals were dark adapted for one hour before the scotopic measurements were started. Mesopic measurements were performed right after the scotopic measurements were completed. For photopic measurements, the animal was light adapted for at least 10 minutes by illuminating the stimulator dome at $30\,cd/m^2$ (photopic strength). For statistical analysis, a-wave and b-wave responses were averaged from five single responses per recording. Data of scotopic ($0.0095\,cds/m^2$, $0.476\,Hz$), mesopic ($3.0\,cds/m^2$, $0.095\,Hz$) and photopic ffERGs ($3.0\,cds/m^2$, $0.625\,Hz$) were analyzed with a linear mixed effects model with point in time, eye, baseline (0d) and interaction between point in time and eye as fixed effects and animals as random effect was

fitted to the data, using unstructured as covariance structure. Test results were considered statistically significant when $p < 0.05$, while we adjusted for multiplicity with Holm-Scheffe procedure. Post-hoc tests compared the treated and untreated eyes for fixed points in time and the points in time among each other separately for both eyes.

Macroscopy

Macroscopic images were taken with a Canon EOS 700D (Canon Inc., Ota, Tokio, Japan) using a macro lens (EF-S60mm f/2.8 MACRO USM) and a mounted ring flash (15 ms-1, Metz mecatech GmbH, Zirndorf, Germany) for uniform illumination.

Hematoxylin and Eosin Stainings

H&E stainings were performed according to the protocol by Rösch et al. [42, 43]. In brief, the eyes were enucleated, punctured twice at the *ora serrata* and fixated for 30 minutes in 4 % paraformaldehyde (PFA) at room temperature (RT). The eyes were transferred to 70 % ethanol and then dehydrated in a tissue dehydration automat (MTM, SLEE, Mainz, Germany) by incubation in a graded alcohol series (2x 70 %, 2x 96 %, and 3x 100 % for 1 hour), followed by xylene (3x 1 hour) and paraffin (4x 1 hour). After that, eyes were embedded in paraffin and 5 µm thick sections were cut with a microtome (Sliding microtome pfm Slide 4003 E, pfm medical AG, Cologne, Germany). Sections were collected in a 50 °C water bath (pfm waterbath 1000, pfm medical AG, Cologne, Germany) and gathered on slides. Sections were then dried overnight at 37 °C, deparaffinated, rehydrated and stained with hematoxylin and eosin. Sections were embedded in Vitro-Clud® (R. Langenbrinck GmbH, Labor- und Medizintechnk, Emmendingen Germany) and pictures were taken with a Leica DM IRB microscope (Leica

Camera AG, Wetzlar, Germany) with a Hitachi HV-C20A camera (Hitachi Ltd., Chiyoda, Tokio, Japan).

Immunohistochemistry

Immunohistochemistry (IHC) stainings were performed according to the protocol by Mataruga et al. [44]. After fixation in 4 % PFA and cryoprotection in sucrose solution the retina was isolated from the eye cup and the irradiated area with surrounding intact tissue cut out. 18 µm thick vertical sections were cut.

The following stainings were used: anti-protein kinase C alpha ($PKC\alpha^{rb}$), anti-calcium binding protein 28K ($CabP^{ms}$), anti-calretinin (Cal^{gt} AB1550), anti-recoverin (Rec^{rb}, Ab5585), anti-HCN1 ($HCN1^{rt}$, RTQ-7C3), anti-rhodopsin (Rho^{ms} 1D4), anti-glial fibrillary acid protein ($GFAP^{ch}$), anti-glutamine synthetase (GS^{ms}), lectin peanut agglutinin (PEA, biotinylated), anti-CD11b ($CD11b^{rt}$), anti-Go-alpha ($Go\alpha^{ms}$), anti-HCN4 ($HCN4^{rt}$ 1A4), anti-PKA RIIb (PKA^{ms}), anti-piccolo ($Piccolo^{gp}$), anti-mGluR6 ($mGluR6^{rb}$). Combinations of used primary and secondary antibodies can be found in the Supplementary Material, Table 3, as well as dilutions and antibody sources.

In some cases, stainings were supplemented with nuclear staining by TO-PRO®3 (TO-PRO®3 Iodide, Thermo Fisher Scientific). TO-PRO®3 (diluted 1:1000) was added to the secondary antibody incubation.

Sections were embedded in Aqua Polymount and examined with a Leica TCS confocal laser scanning microscope (Leica Microsystems, Heidelberg, Germany) with oil immersion lenses (x63/1.4). Different fluorescence channels were scanned sequentially to minimize crosstalk. Images of single confocal planes or stacks of images collapsed in the maximum projection mode were processed in ImageJ (ImageJ 1.45s, Wayne Rasband, National Institutes of Health, USA; RRID:SCR_003070) with the Bio-Formats add-on (ImageJ 1.45s; Bioformats

5.0.4; RRID:SCR_000450).

MEA Recordings

The "tissue preparation" and "MEA recordings and electrical stimulation" protocols from Haselier et al. were followed [45], except that the poly-D-lysine hydrobromide treatment was not performed. Stimulus parameters used and respective responses can be found in the Supplementary Material.

The MEA with the attached retina was placed in the MEA2100-System (Multi Channel Systems MCS GmbH). The retina was immediately perfused with constantly carbogenated AMES' medium at a perfusion rate of 3-4 ml/min with a $VC^{(3)}$-perfusion system (ALA Scientific Instruments, Farmingdale, NY, USA) and a peristaltic pump (Gilson Inc., Middleton, WI, USA). Recordings were started after an acclimatization phase of 20 minutes minimum.

MEA Analysis

Oscillations: For the evaluation of oscillatory potentials, a 50 Hz lowpass filter was applied to the raw data in MC-Rack. Files were then converted to a .txt file with the MC-DataTool (2.6.15, Multi Channel Systems MCS GmbH, Reutlingen, Germany). A Fast Fourier Transformation (FFT) was performed with a custom MATLAB (R2016a, The MathWorks Inc., Natick, MA, USA) script (written by Dr. Janis Brusius, Institute of Complex Systems 8, Forschungszentrum Jülich, Germany). Dominant frequencies of one animal, measured at different electrodes, were taken into account for the calculation of a median. The medians of single animals from one group (5d, 6w, 8w, 12w, respectively; one median per animal) were then treated as single measurements and used for unpaired t-tests to compare the four groups (5d, 6w, 8w, 12w).

Results

Ray Tracing Simulation

Measurements of the UV LED array at different distances revealed intensities between 2 mW/cm² at 10 cm distance and 12.5 mW/cm² at 1 cm distance. For the simulation with the inserted lens (Figure 2 A), a distance of 1 mm from the LED casing and 10 mm from the mouse cornea resulted in a homogenous illumination of about 25 % of the whole retina (Figure 2 C), being the best possible outcome with standard lenses tested. Note that absorption of ocular media (cornea, aqueous humour, lens, vitreous humour) was not accounted for in ray tracing simulations.

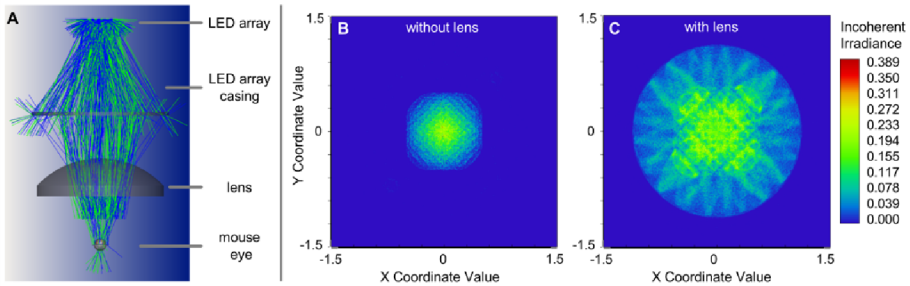

Figure 2: Ray tracing simulation with LED array and mouse eye. **A**: Ray tracing alignment. Note that the illustration is not drawn to scale. Distance from LED-casing to lens: 1 mm; thickness lens: 9 mm; distance from lens to cornea: 10 mm. **B** and **C**: Retinal surface illumination without lens (B) and with lens (C). X and Y coordinate values state the distance from the optical axis in mm. Color scale states the power on the retinal surface, starting with blue (0.000 incoherent irradiance) and increasing to red (0.389 incoherent irradiance).

Dose Escalation Study

The dose escalation study taught us that, with rising dosage, the diameter of the irradiated area of the retina increased, yet no notable additional damage was induced in other retinal layers, as shown in Figure 3 A, B, as well as Figure

4. This could be observed in sd-OCT scans as well as in H&E stainings. Based on H&E stainings, sd-OCT InRe images and MEA recordings from irradiated retinae, the diameter of the irradiated retinal area was estimated to be approx. 1500 µm at dosages between 6.5 J/cm² and 9.3 J/cm². The light beam was not always exactly centered on the optic nerve head, which was especially visible at lower dosages where the diameter of the degenerated area was smaller (see Figure 3 A).

Since we did not want to risk damage to the inner retinal layers and/or the RPE with even higher dosages [46, 47, 33] but rather aimed for a large area with degenerated PRs we decided that the ideal dosage of UV radiation lay between 6.5 J/cm² and 9.3 J/cm², primarily based on H&E stainings, that allowed the most detailed impression. Hence, we performed irradiations in the characterization study with 7.5 J/cm².

We found that neovascularization of the cornea could arise if the eye was moisturized with saline during irradiation. The treatment of neovascularization with Isopto-MAX® eye ointment did not always lead to an improvement, probably due to the fact that the mice were trying to clean off the ointment immediately after application, thereby further irritating the eye. Neovascularization of the mouse cornea after UV irradiation has been observed before by Vangsted, who reported that long-term irradiation with a maximum dosage of 320 J/cm² led to a similar effect as observed in our dose escalation study [48]. Occurrence of neovascularization was not dependent on UV dosage (Figure 3 C-F), thus, we assumed that the precorneal film could not be maintained sufficiently by saline application. Dry eye is known to lead to neovascularization [49].

In the following experiments, Methocel® – that has a very similar refractive index as the cornea (Methocel®: 1.336 [50]; mouse cornea: 1.3 [40]) – was

chosen for moisturizing the eye during irradiation. Methocel® application every two to three minutes proved to be sufficient to avoid neovascularization (see Figure 3 F).

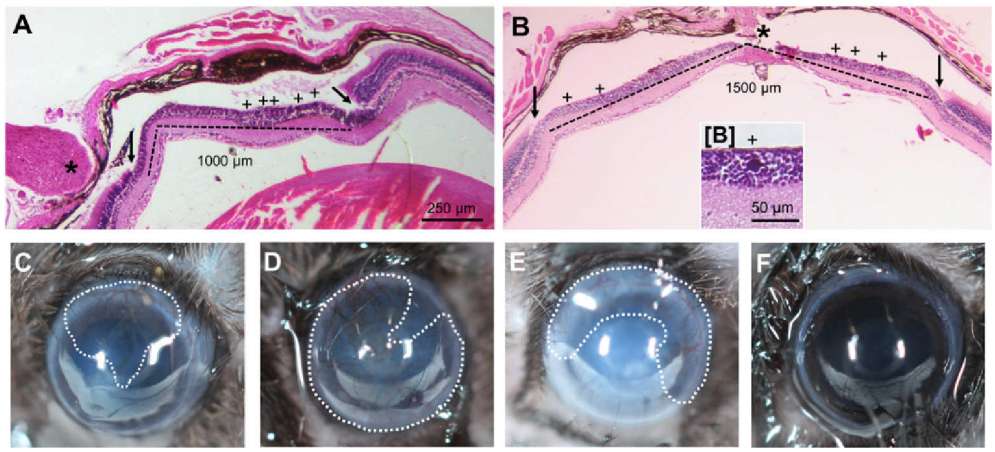

Figure 3: Dose escalation study: H&E stainings and macroscopic images.
A and B: H&E stainings of eyes irradiated with 2.8 J/cm² (A) and 9.3 J/cm² (B). * = optic nerve head; arrows indicate transition from intact to irradiated area; crosses mark positions of "basophilic inclusions" (see insert [B]: higher magnification of a "basophilic inclusion" in another position); dashed line = width of irradiated area: approx. 1000 µm in A, approx. 1500 µm in B. **C,D,E,F**: macroscopic images of eyes irradiated with 5.6 (C), 9.0 (D), 9.3 (E) and 7.5 J/cm² (F) 4 weeks after irradiation. Dashed lines encircle neovascularized areas (C,D,E). Macroscopic images C, D and E are from the dose escalation study (eyes were moisturized with saline during irradiation), image F shows an eye from the characterization study (eyes were moisturized with Methocel® during irradiation). No neovascularization was observed under these conditions.

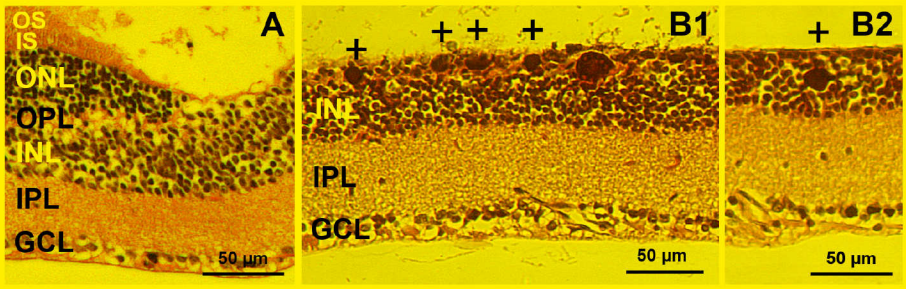

Figure 4: High magnification HE stainings of the retinal layers of treated eyes of the dose escalation study.
HE staining of eyes irradiated with 2.8 J/cm² (A) and 9.3 J/cm² (B). The images correspond to the same animals as depicted in Figure 3 A and B. OS = outer segments, IS = inner segments, ONL = outer nuclear layer, OPL = outer plexiform layer, INL = inner nuclear layer, IPL = inner plexiform layer, GCL = ganglion cell layer

Spectral domain Optical Coherence Tomography

In sd-OCT scans, we were able to follow the progression of the degeneration process. Please note that for measurements at 1d, 2d and 4d only one animal was examined each. These points in time only served to find the point in time where about 50 % of photoreceptors were gone. Although the data of those animals is not reliable (n=1), it is described here and included in Figure 5 A as exemplary data.

One day after irradiation, the effect of UV irradiation was already visible. As shown in Figure 5, in InRe as well as in cross-sectional (CS) images the transition from intact to irradiated areas could be readily identified and stayed visible until the maximum observation period of 12 weeks (12w). One day (1d) after irradiation the retina appeared thicker than in control conditions, due to a swelling of the outer nuclear layer (ONL). After two (2d) and four days (4d) swelling was still visible, but less pronounced, until at five days (5d) about 50 % of the PRs were gone. We could not decide from sd-OCT scans whether the increase in thickness was due to a swelling of PR somata

or due to the infiltration of the ONL by microglia that was observed in IHC (see Supplementary Material, Figure 12). One week (1w) after irradiation, only some residual cells were found in the ONL. The ONL had completely disappeared after two weeks (2w). Over the course of the following weeks, no more changes were observed in sd-OCT scans (see Figure 5).

Statistics of whole-retina thickness measurements confirmed what was found in sd-OCT images. Retinal thickness of untreated eyes did not change over the course of 12 weeks. In the treated eye, retinal thickness at 5d and 1w was significantly greater than at all later points in time, respectively. The multivariable analysis revealed that all tested covariables point in time, eye, baseline, and interaction between point in time and eye had a statistically significant effect on the outcome sd-OCT (see Table 1). The conducted post-hoc tests comparing treated and untreated eyes for fixed points in time and comparing points in time separately for each eye revealed that there are significant differences for all comparisons between treated and untreated eyes at the same point in time. In the comparison of 5d with later points in time in the treated eye, significant differences were found for all comparisons. Comparing 1w with 2w and 4w in the treated eye suggested significant differences as well. In contrast to that, comparisons between later points in time within treated eyes revealed no significant differences. All comparisons with exact p-values (after Scheffe adjustment) are stated in Supplementary Material Table 3-2. The mean retinal thickness of untreated eyes of all individuals over all points in time was 215 µm ± 3.8 µm. In treated eyes, the mean thickness declined to 161 µm ± 15.7 µm at 5d, further decreased to 128 µm ± 4.8 µm at 1w and stabilized at 108 µm ± 5.0 µm at 2w (Figure 5).

The multivariable analysis of inner retina thickness measurements revealed

that all tested covariables point in time, eye, baseline, and interaction between point in time and eye had a statistically significant effect on the outcome sd-OCT (see Table 1). The conducted post-hoc tests comparing treated and untreated eyes for fixed points in time and comparing points in time separately for each eye revealed that there are significant differences for 6w and 8w between treated and untreated eyes at the same point in time. Comparing 5d with 6w in the treated eye suggested significant differences as well. In contrast to that, comparisons between other points in time within treated eyes revealed no significant differences. All comparisons with exact p-values (after Scheffe adjustment) are stated in Supplementary Material Table 3-2. The mean inner retinal thickness of untreated eyes of all individuals over all points in time was 112 µm ± 2.6 µm. In treated eyes, the mean thickness developed over 112 µm ± 1.4 µm at 5d, 113 µm ± 1.3 µm at 1w, 108 µm ± 1.3 µm at 2w, 109 µm ± 1.3 µm at 4w, 103 µm ± 1.3 µm at 6w, 106 µm ± 0.9 µm at 8w to 107 µm ± 1.3 µm at 12w (Figure 6).

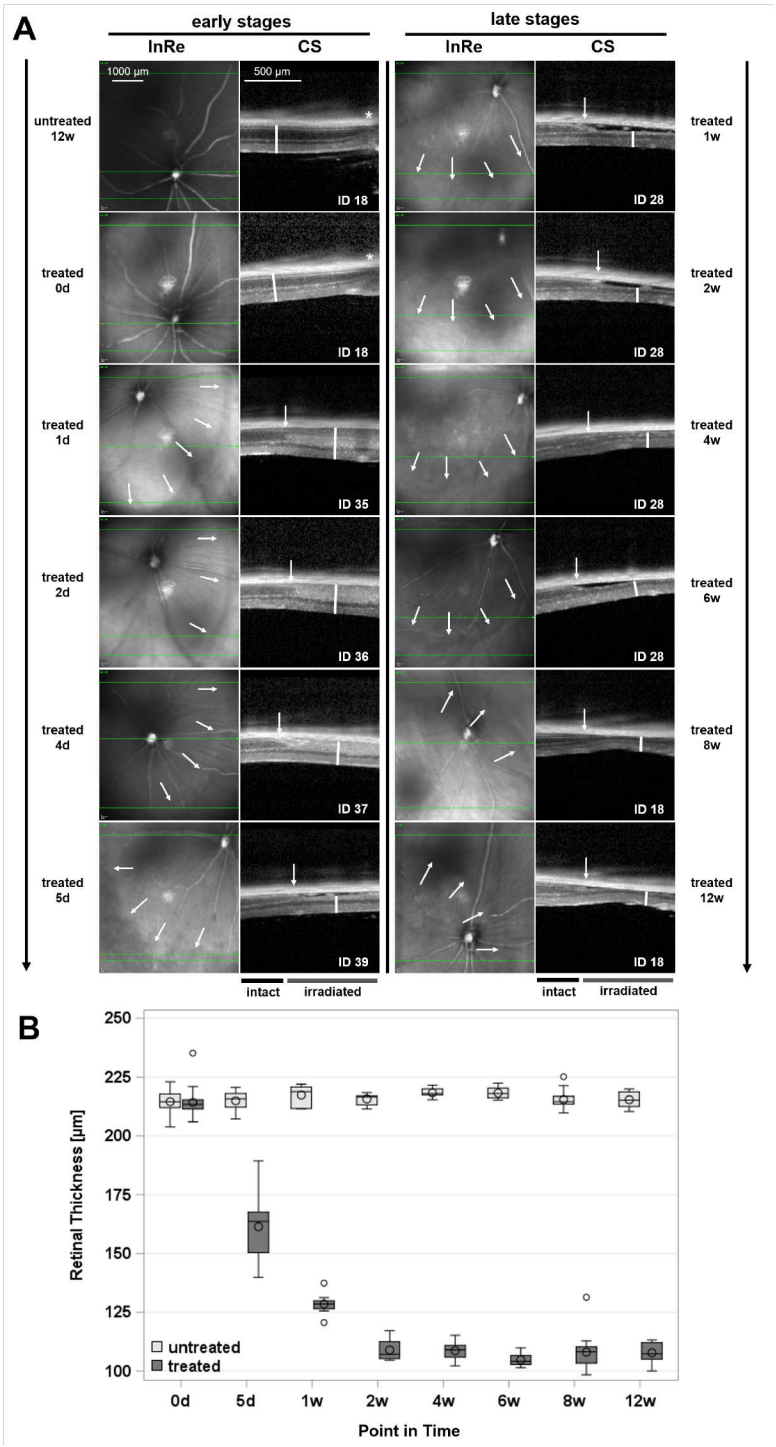

Figure 5: Time course of PR degeneration after irradiation with 7.5 J/cm². Cont. on next page...

Figure 5: ...cont. from previous page
A: sd-OCT scans at different points in time. InRe and CS images in left (early stages) and right (late stages) columns, respectively. InRe and CS images shown side by side are from the same animal at one specific point in time. In treated eyes, the intact area in CS images is displayed in the left part of the image, the irradiated area in the right part. White arrows indicate the transition from intact to irradiated areas, white bars indicate retinal thickness. Animal IDs allow assignment of scans to individual animals. **B**: sd-OCT thickness measurements. Measurements from untreated (light grey) and treated (dark grey) eyes at different points in time were compared. Before irradiation (0d, baseline) n = 30 untreated eyes and n = 31 treated eyes were included. 5d after irradiation: n = 7 untreated and treated eyes; 1w, 2w, 4w and 6w after irradiation: n = 7 untreated eyes, n = 8 treated eyes; 8w after irradiation: n = 16 untreated and treated eyes; 12w after irradiation: n = 8 untreated and treated eyes; Points in time covered by more than one of the four experimental groups show cumulated data of combined groups. Data were not cumulated for statistical analysis, but statistical tests were performed with separate groups. **** $p \leq 0.0001$; ns = not significant. Exact p-values (after Scheffe adjustment) are stated in Supplementary Material Table 3-2.

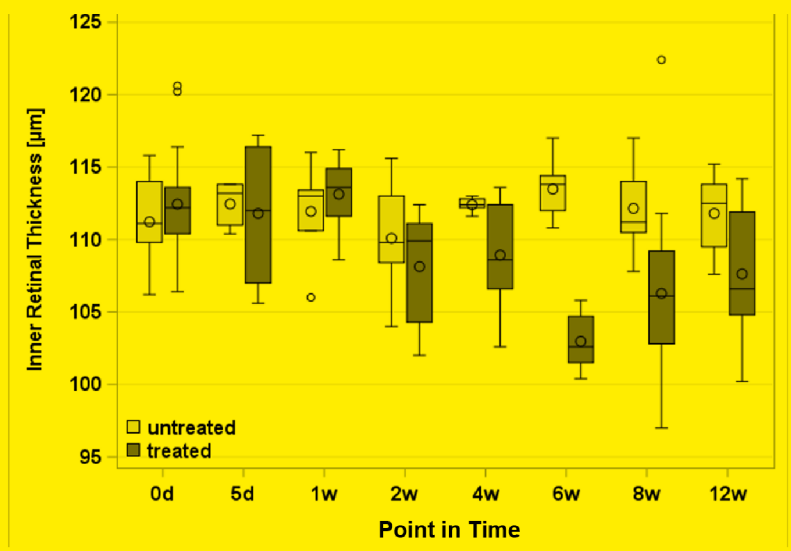

Figure 6: Thickness of the inner retina after irradiation with 7.5 J/cm². Cont. on next page...

Figure 6: ...cont. from previous page
B: sd-OCT thickness measurements of the inner retina. Measurements from untreated (light grey) and treated (dark grey) eyes at different points in time were compared. Before irradiation (0d, baseline) n = 30 untreated eyes and n = 31 treated eyes were included. 5d after irradiation: n = 7 untreated and treated eyes; 1w, 2w, 4w and 6w after irradiation: n = 7 untreated eyes, n = 8 treated eyes; 8w after irradiation: n = 16 untreated and treated eyes; 12w after irradiation: n = 8 untreated and treated eyes; Points in time covered by more than one of the four experimental groups show cumulated data of combined groups. Data were not cumulated for statistical analysis, but statistical tests were performed with separate groups. Exact p-values (after Scheffe adjustment) are stated in Supplementary Material Table 3-2.

	Effect	DF	p-value
Overall thickness	Point in time	6	< 0.0001
	Eye	1	< 0.0001
	Baseline	1	0.0131
	Point in time * Eye	6	< 0.0001
Inner thickness	Point in time	6	0.0040
	Eye	1	< 0.0001
	Baseline	1	0.0193
	Point in time * Eye	6	0.0003

Table 1: Type 3 tests of fixed effects for sd-OCT measurements - multivariable analysis
The different points in time, as well as both eyes and the interaction between point in time and eye differ significantly according to type 3 tests of fixed effects. Overall thickness refers to thickness measurements of the whole retine, inner thickness refers to thickness measurements of the inner retina only.
DF = degrees of freedom.

Full-field Electroretinography

Please note that for measurements at 1d, 2d and 4d only one animal was examined each. These points in time only served to find the point in time where about 50 % of photoreceptors were gone. Although the data of those animals is not reliable (n=1), it is described here as exemplary data.

FfERG recordings revealed deterioration of a- and b-wave responses as soon as 1d after UV irradiation (data not shown). For scotopic and photopic ffERGs,

only b-wave responses were evaluated, since a-wave responses were barely detectable. For mesopic ffERGs, a- and b-wave responses were analyzed.

The rod driven response of ON-bipolar cells, as represented by the b-waves under scotopic conditions [51], was reduced at all points in time after irradiation. However, even 12w after irradiation, a small response persisted that most likely originated from the non-irradiated retina (Figure 7 A, B).

The mesopic response represents a rod-dominated combined signal from PRs (a-wave) and ON-bipolar cells of both, rod and cone system (b-wave) [52] (Figure 7 A, C1, C2).

Photopic responses represent cone activity, with a-waves representing cones with post-receptoral ON-bipolar cells (b-waves) [52]. A-waves were very small or undetectable in our data and therefore not further evaluated (Figure 7 A, D).

An unexpected feature was the drop in a- and b-waves in both treated and untreated eyes 5d after irradiation, with amplitudes considerably lower than at later points in time (Figure 7 B, C1, C2). There also was the tendency for amplitudes of untreated eyes to slightly decrease over the course of twelve weeks.

The multivariable analysis revealed that the tested covariables point in time, eye, and interaction between point in time and eye had a statistically significant effect on the outcome ffERG for scotopic and mesopic ffERGs. The tested covariable baseline was only significant for scotopic b-wave, but not for photopic b-wave or mesopic a- and b-wave (see Table 2). The conducted post-hoc tests comparing treated and untreated eyes for fixed points in time and comparing points in time separately for each eye suggested significant differences for all comparisons between treated and untreated eyes at the same point in time (exception: 12w in photopic measurements). In the comparison of 5d and 1w in the untreated eye, a significant difference was found as well (exception: photopic measurements), but all other comparisons suggested that there are no signifi-

cant differences. All comparisons with exact p-values (after Scheffe adjustment) are stated in Supplementary Material Table 4-2.

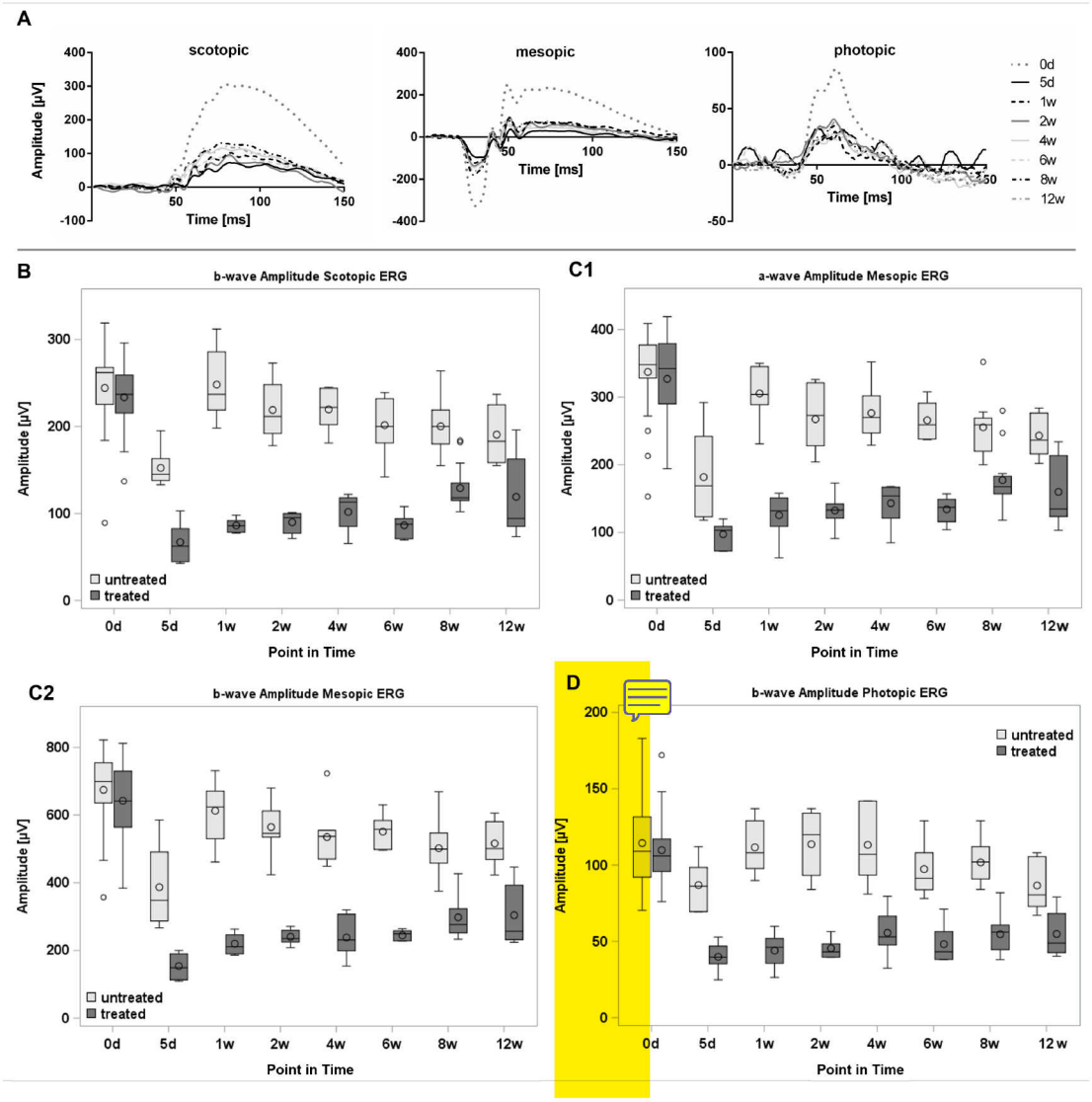

Figure 7: Development of a- and b-wave amplitudes from ffERG recordings over 12w after irradiation with 7.5 J/cm².
A: Averaged scotopic, mesopic and photopic responses are depicted. Grey dotted traces represent control conditions (treated eye before irradiation, 0d), the other traces represent points in time of treated eyes after irradiation: 5d, 1w, 2w, 4w, 6w, 8w, 12w. B-D: a- and b-wave amplitudes from treated (dark grey) and untreated (light grey) eyes at different points in time. Points in time covered by more than one of the four experimental groups (0d and 8w) show cumulated data of combined groups. Data were not cumulated for statistical analysis, but statistical tests were performed with separate groups.

Figure 7: ...cont. from previous page
B: Before irradiation (0d, baseline) n = 28 untreated and treated eyes were included, each. 5d, 4w and 6w after irradiation: n = 7 untreated and treated eyes; 1w and 2w after irradiation: n = 6 untreated and treated eyes; 8w after irradiation: n = 14 untreated and treated eyes; 12w after irradiation: n = 8 untreated and treated eyes; **C1 and C2**: 0d, baseline: n = 30 untreated and treated eyes; 5d, 1w, 2w, 4w, and 6w after irradiation: n = 7 untreated and treated eyes; 8w after irradiation: n = 14 untreated and treated eyes; 12w after irradiation: n = 8 untreated and treated eyes. **D**: 0d, baseline: n = 28 untreated and n = 27 treated eyes were included. 5d after irradiation: n = 6 untreated and treated eyes; 1w after irradiation: n = 6 untreated and n = 7 treated eyes; 2w after irradiation: n = 5 untreated and treated eyes; 4w and 6w after irradiation: n = 7 untreated and treated eyes; 8w after irradiation: n = 11 untreated and treated eyes; 12w after irradiation: n = 8 untreated and treated eyes; No significant differences were found in comparisons between points in time of untreated eyes, except for the comparison 5d vs. 1w. Within treated eyes, no significant differences were found between the different points in time (ignoring baseline, 0d). Untreated and treated eyes did not differ at 0d (baseline), but showed significant differences at all other points in time. Different animal numbers for the recordings were the result of disturbances during single measurements. Those recordings were excluded from the data set and therefore altered the animal numbers. **** $p \leq 0.0001$; *** $p \leq 0.001$; ** $p \leq 0.01$; * $p \leq 0.05$; ns $p > 0.05$. Exact p-values (after Scheffe adjustment) are stated in Supplementary Material Table 4-2.

ERG	Effect	DF	p-value
b-wave scotopic	Point in time	6	0.0004
b-wave scotopic	Eye	1	< 0.0001
b-wave scotopic	Baseline	1	0.0099
b-wave scotopic	Point in time * Eye	6	< 0.0001
a-wave mesopic	Point in time	6	0.0016
a-wave mesopic	Eye	1	< 0.0001
a-wave mesopic	Baseline	1	0.5239
a-wave mesopic	Point in time * Eye	6	< 0.0001
b-wave mesopic	Point in time	6	0.0006
b-wave mesopic	Eye	1	< 0.0001
b-wave mesopic	Baseline	1	0.3580
b-wave mesopic	Point in time * Eye	6	0.0003
b-wave photopic	Point in time	6	0.2284
b-wave photopic	Eye	1	< 0.0001
b-wave photopic	Baseline	1	0.6126
b-wave photopic	Point in time * Eye	6	< 0.0567

Table 2: Type 3 tests of fixed effects for ERG measurements - multivariable analysis
The different points in time, as well as both eyes and the interaction between point in time and eye differ significantly according to type 3 tests of fixed effects. DF = degrees of freedom.

Immunohistochemistry

In general, the time course of PR degeneration observed in IHC matched that observed in sd-OCT. Furthermore, in none of the stainings we detected clear differences between sections from 6w, 8w and 12w, indicating that most of the remodeling process is completed 6w after irradiation at the latest and that only minor changes might occur later on.

Please note that for measurements at 1d, 2d and 4d only one animal was examined each. Although the data of those animals is not reliable (n=1), it is described here as exemplary data.

Stainings shown in Figure 8 were performed with the same antibody combinations that we have used in previous work on retinae of rd10 mouse [42] and

of MNU-treated mice [43], enabling us to compare the histology of the three models.

We observed a sharp transition between irradiated and non-irradiated retina 5d after irradiation (Figure 8, arrow). In the irradiated area, the ONL was strongly reduced in thickness and no intact outer segments (OSs) were observed in the staining against recoverin and rhodopsin (green, blue). Only some remains of rod OSs and end feet were found (green). In TO-PRO®3 stainings (labeling of nucleic acids) 5d after irradiation the nuclei of remaining PRs looked altered (data not shown), probably due to DNA disorganization, induced by oxidative stress (see discussion).

GFAP immmunoreactivity (Figure 8, green) revealed that Müller cells were reactive, typical for the onset of PR degeneration. In short term retinae (1-5 days after irradiation), the tissue appeared softer and more vulnerable, compared to later stages, making preparation and sectioning difficult (note that tissue preservation was not optimal in the 5d sections: The tissue was fixed just as the samples of later points in time, but was more difficult to handle as it was softer and more unstable).

At 6w, in the treated area, rod bipolar cells (anti-PKCα, green) had lost their dendrites but seemed otherwise intact, amacrine cells labeled against calretinin (blue) seemed normal (Figure 8). The characteristic stratification observed in the calretinin staining (three bands in the inner plexiform layer (IPL)) was preserved in irradiated retinae at all points in time (5d and 6w in Figure 8). Horizontal cells (strongly magenta labeled cells at the outer margin of the Inner Nuclear Layer (INL)) were missing in the irradiated area. Only punctate recoverin staining was observed while rod OSs labeled against rhodopsin and recoverin appeared healthy in the neighboring untreated area (Figure 8). Müller cell reactivity was over, indicated by their low GFAP expression.

We detected large round structures that we called "basophilic inclusions" based on their appearance in H&E stainings (see Figure 3 A, B, [B], crosses). They were located in the outermost row of the INL, reminiscent of swollen somata (asterisks in Figure 9 B, C). They appeared blue in H&E stainings and were completely labeled by TO-PRO®3, suggesting that they contained DNA, however, no nucleus could be identified. The structures were circular and up to five times the size of bipolar cell somata (compare bipolar cells and "basophilic inclusions" in Figure 9 C). They were not labeled with antibodies against recoverin (PRs) or CabP (horizontal cells), persisted for at least up to 12w after irradiation and did not seem to change in size, shape or position.

Figure 9 A shows a staining of rod bipolar cells (anti-PKCα, green) and all ON bipolar cells (anti-Goα, magenta) 6w after irradiation. In the irradiated area, bipolar cell dendrites were missing. In the immediate neighborhood of the intact area, dendrites of ON bipolar cells were strongly elongated (arrows) indicating a reaction of bipolar cells close to the transition zone. We did not observe this effect in type 3a and type 3b OFF cone bipolar cells.

Figure 9 D-E shows the organization of PR end feet. In untreated retina, three components can be observed at each rod end foot (anti-PSD95, blue: plasma membrane; anti-piccolo, magenta: ribbon; anti-mGluR6, green: mGluR6 on postsynaptic bipolar cell dendrites). 5d after irradiation, only a small fraction of synapses was left. While some endfeet still appeared normal, others were disorganized.

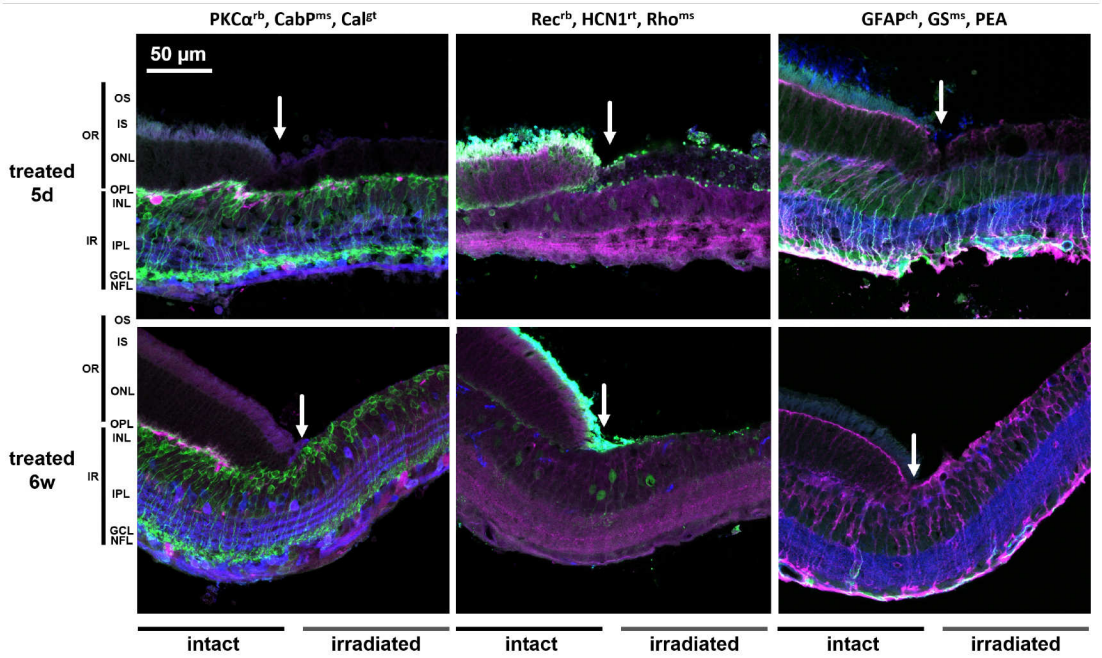

Figure 8: IHC stainings 5d and 6w after irradiation with 7.5 J/cm² at the transition zones between irradiated and non-irradiated retina. All images depict parts of the retina where the transition from intact (left part of each picture) to irradiated (right part of each picture) areas of the retina is visible. Arrows indicate location of transition. Left column: anti-PKCα (green, rod bipolar cells), anti-CabP (magenta, horizontal cells), anti-Calretinin (blue, amacrine cells). Middle column: anti-Recoverin (green, PRs, type 2 bipolar cells), anti-HCN1 (magenta, PR somata, inner segment (IS), IPL processes), anti-Rhodopsin (blue, rod OS). Right column: anti-GFAP (green, astrocytes and reactive Müller cells), anti-GS (magenta, Müller cells), anti-PEA (blue, cone end feet, cone IS and OS. Top row: treated eye, five days (5d) after irradiation; bottom row: treated eye six weeks (6w) after irradiation – both from the characterization study.
OR = outer retina, IR = inner retina, OS = outer segments, IS = inner segments, OPL = outer plexiform layer, INL = inner nuclear layer, IPL = inner plexiform layer, GCL = ganglion cell layer, NFL = nerve fiber layer.

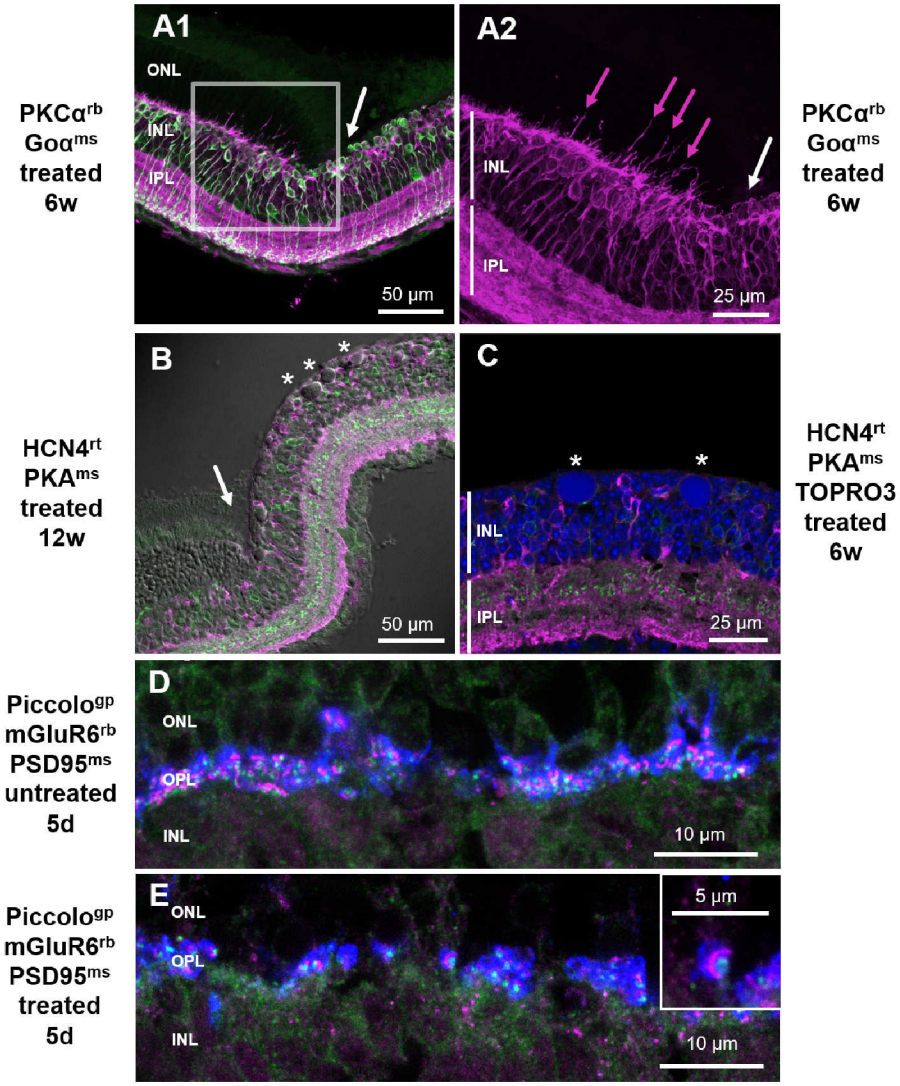

Figure 9: IHC stainings from retinae of the characterization study (7.5 J/cm²).
Anti-PKCα (green, rod bipolar cells), anti-Goα (magenta, all ON-bipolar cells and dendritic tips). Anti-HCN4 (green, somata and axon terminals of type 3A cone bipolar cells), anti-PKA RIIb (magenta, type 3B cone bipolar cells), TO-PRO®3 (blue, nucleic acids, nucleus). Anti-piccolo (magenta, ribbon, PRs), anti-mGluR6 (green, dendritic tips of rod bipolar cells and all ON bipolar cells), anti-PSD95 (blue, rod endfeet).**A1**: treated eye 6w after irradiation; **A2**: magenta channel of A1 (grey frame) at higher magnification; **B**: treated eye, 12w after irradiation with brightfield; Cont. on next page...

Figure 9: ...cont. from previous page
C: treated eye 6w after irradiation; **D**: untreated eye 5d after irradiation; **E**: treated eye 5d after irradiation.
Abbreviations as in Figure 8. White arrows indicate location of transition from intact to irradiated retina, where both are present in one picture. Asterisks indicate positions of "basophilic inclusions". Magenta arrows highlight dendrites of bipolar cells..

MEA Recordings

In the isolated retina, the irradiated area could be readily distinguished from normal retina by sight (Figure 10 A-C). The electrophysiological recordings of spontaneous activity revealed a strikingly clear transition from irradiated to non-irradiated areas (Figure 10 D). While the intact areas showed activity typical for wildtype (WT) retina, irradiated areas displayed oscillations similar to those observed in rd1 or rd10 retina [53, 54, 55, 56] (Figure 10 D, E). For a direct comparison, see Supplementary Material Figure 13.

We observed mean oscillatory frequencies of 6.0 Hz at 5d, 4.8 Hz at 6w, 5.1 Hz at 8w and 5.0 Hz at 12w after irradiation. The cumulated mean of all groups was 5.2 Hz (Figure 10 F). A significant difference was only found between oscillatory frequencies at 5d, compared with frequencies at 6w. Retinae of treated eyes were also tested for light-evoked and electrically-evoked responses (see Supplementary Material).

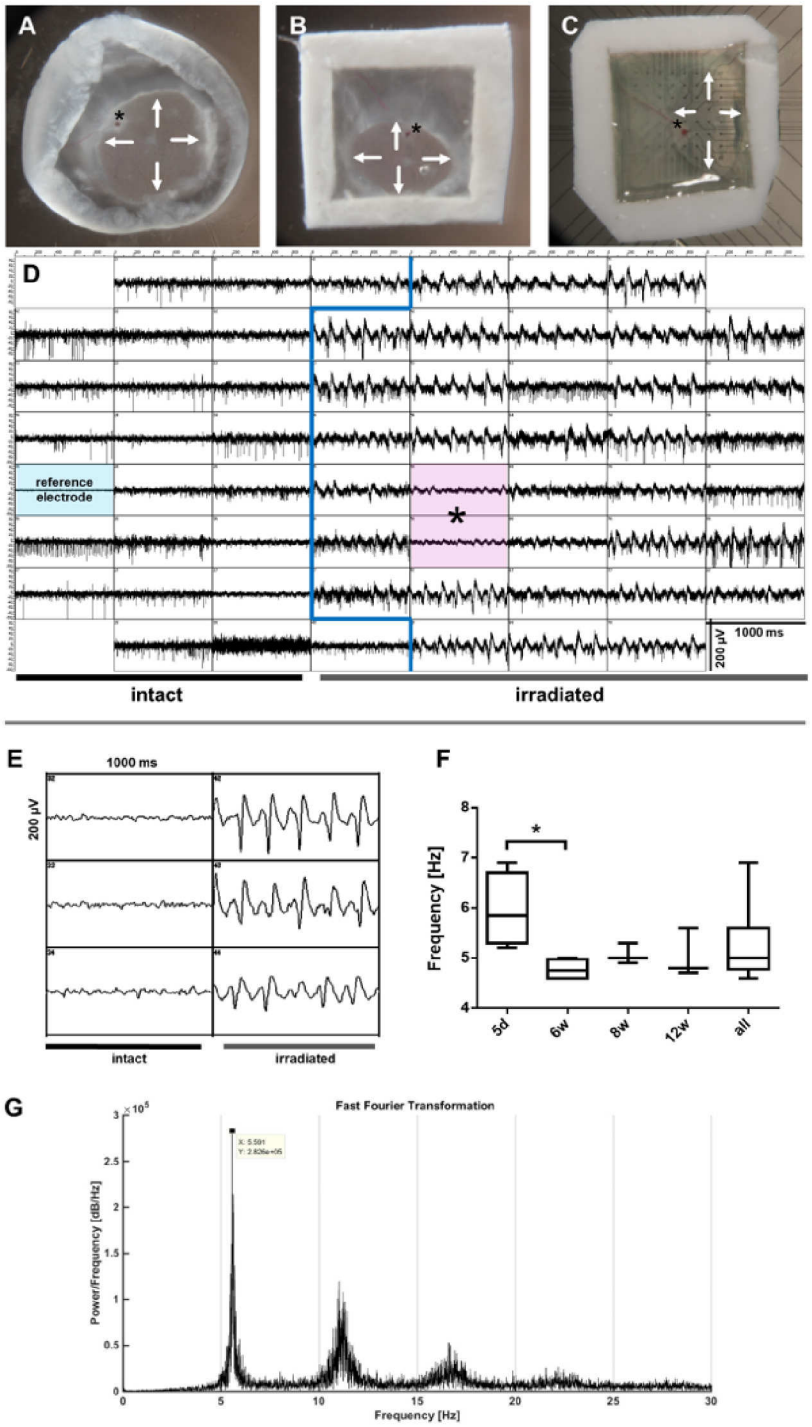

Figure 10: MEA recording of an irradiated retina 12 weeks after irradiation and FFT analysis of oscillations (7.5 J/cm²). Cont. on next page...

Figure 10: ...cont. from previous page
A: isolated retina with vitreous removed. **B**: isolated retina attached to nitrocellulose paper frame. **C**: isolated retina on frame attached to MEA (ganglion cells facing electrodes). Arrows in A, B and C indicate the border of the irradiated retinal area. **D**: raw data of MEA recording. Blue line indicates border between electrodes covered with intact area (left) and irradiated area (right). Asterisks indicate electrodes covering the optic nerve head. **E**: 50 Hz lowpass filtered data of the recording depicted in D, left column with electrodes from intact area, right column with electrodes from irradiated area. **F,G**: FFT analysis (G) of irradiated area and box-whisker plot and statistical analysis (F) of dominant oscillatory frequencies from retinae isolated 5d, 6w, 8w and 12w after irradiation; all = cumulated data of all four groups; unpaired t-test was performed to compare groups; * $p \leq 0.05$. Only significant differences were visualized, all other comparisons were not significant.

Discussion

We aim for the establishment of a UV-induced PR degeneration model in the rabbit to provide for a unilateral large-eye model of RP. As a first step, we established and characterized such a model in the mouse, allowing for a direct comparison with the genetic mouse model rd10, which is an acknowledged model for RP.

Please note that the results presented here were obtained from female mice only. It is possible that there is a gender specific effect that we missed due to our experimental setup.

In general, irradiated areas of treated eyes showed very similar characteristics as rd10 retinae in sd-OCT scans, IHC, and MEA recordings (compare [42, 57, 58, 55]).

A striking feature of the UV-induced model was the sharp border between degenerated and intact areas of the retina in treated eyes. This was observed

both on the anatomical and the electrophysiological level. One might have expected a smooth transition from intact to irradiated areas with decreasing layers of PRs in between, as the intensity of the UV light decreases from center to periphery (Figure 2 C). Cideciyan et al. observed a similar effect of abrupt transition in their light exposed retinae of rhodopsin mutant dogs [21]. One explanation would be a threshold effect that allows degeneration of PRs only, if surpassed. PRs may be particularly susceptible to toxic intensities of UV light because of their high metabolic rate [59]. The high oxidative metabolism could make PRs more vulnerable to oxidative stress, since a higher amount of reactive oxygen species would be present. Reactive oxygen species are abundant in UV exposed cells [60] and are known to have deleterious effects on a variety of cells [61, 62, 63] *via* diverse mechanisms [64, 65, 66].

In ffERG recordings, we observed a reduction, but not an elimination of both a- and b-wave upon irradiation, as expected. The decline of the responses was very abrupt and fast, unlike in RP, where the responses slowly decline over time. Unexpectedly, we also found a considerable transient drop in a- and b-wave amplitude 5d after irradiation in both treated and untreated eye. The drop was consistently observed in seven animals, making a random event unlikely. As of now, we do not have a sufficiently supported theory what the cause of this event might be, but a bilateral inflammatory response could explain the drop in amplitude [67]. This is supported by the fact that hyperreflectivity in sd-OCT and the transient drop in ffERG responses occurred simultaneously. There also was the tendency for amplitudes of untreated eyes to slightly decrease over the course of twelve weeks. This might be an aging effect, as shown by Rösch et al. [42]. Our animals from the 12 week group were 9.1 $\pm$ 1.2 weeks old at the time of irradiation, hence they were 21.1 $\pm$ 1.2 weeks

old at 12 weeks after irradiation. The decline in amplitude in ffERG recordings in Rösch's work took place between postnatal week 12 and 24, coinciding with the slight decrease in amplitude in control eyes of our study.

While PRs degenerated within a short time after irradiation, no major changes were observed in other cell types, except for the rapid loss of horizontal cells in the UV-induced model (Figure 8). In the rd10 mouse, horizontal cells remain intact up to PNW 24 [42], but at nine months of age, approx. 29 % of horizontal cell somata are lost [57]. In the MNU-induced model, a difference in horizontal cell survival was found between intraperitoneal and intravitreal injection: After systemic administration of MNU and subsequent death of PRs, horizontal cells lost their dendrites, but stayed intact otherwise. After intravitreal application, horizontal cells disappeared completely at those retinal sites, at which PRs had completely degenerated [43]. Probably, horizontal cells are more susceptive to neurotoxic situations than other retinal cells. We cannot rule out that, besides the loss of synaptic input, direct effects, e.g., oxidative stress, affect the survival of horizontal cells.

We can only speculate about the nature of the "basophilic inclusions", since we did not focus on their detailed characterization. They were not living cells, since we could not find nuclei within them. It is tempting to speculate that they originated from dead horizontal cells or PRs, yet they were negative for CabP and recoverin. However, we cannot rule out that these markers were degraded during degeneration. Cideciyan et al. discovered similar structures (termed "pyknotic nuclei") in their light exposed rhodopsin mutant dog retinae [21].

Our MEA recordings revealed a pathological oscillatory activity in irradiated retinal areas. The frequencies observed here are in line with studies describing frequencies in other models of RP. In rd10 recordings, frequencies around 4 Hz were observed in retinae of animals aged 4-12 months, while 6 Hz were recorded in retinae of animals aged 1-3 months [53]. In the MNU-induced model of PR degeneration, oscillatory frequencies of 4-6 Hz or 3-9 Hz [58, 45] were found. In rd1 retina, frequencies were reported to be in the range of 10 Hz [54].
Interestingly, the sharp contour between intact and irradiated retina was not only detected on a microscopic/histological level, but also on an electrophysiological level, as measured with MEAs consisting of electrodes that were 200 µm apart. While we cannot rule out a smoother transition that escaped our spatial sampling, we should point out that 200 µm resolution lies in the physiological range of ganglion cell receptive field sizes [68, 69]. There is circumstantial evidence that oscillatory waves may travel in rd10 retina [53]. The sharp transition would indicate that the pathological activity in the degenerated area cannot spread across the border into the healthy part of the retina, neither can activity from the healthy region spread into the degenerated area and, thereby, suppress pathological activity.

In summary, UV irradiation of the female mouse eye with 7.5 J/cm^2 leads to a reliable PR degeneration without substantially harming other ocular tissues. The UV-induced model resembles the well characterized rd10 mouse model in both morphological and electrophysiological properties, as measured in MEA recordings. The slow decline of electrophysiological responses over time to ffERG stimuli typical for RP could not be observed in our model, but instead the ffERG responses dropped shortly after irradiation. With a few reservations, the model presented here can serve as a model for end stage RP, with the advantage of

an intraindividual control eye. However, it must be pointed out that using our experimental setup, only a part of the retina could be irradiated with UV light. By improving the custom optical apparatus, a larger retinal area might be targeted.

In a next step, this method of UV irradiation will be transferred to the rabbit, to obtain a large-eye animal model. The challenge will be, to find a suitable dosage for this species, as the rabbit's ocular media are qualitatively very different from those of the mouse. Cornea and lens transmit lower amounts of UV light [70, 71, 72, 73, 74], and the susceptibility of the rabbit's retina could be different as well.

Acknowledgements

Ray tracing simulations were conducted in collaboration with: Prof. Dr. rer. nat. Loosen and M.Sc. Lasse Büsing; Chair for Technology of Optical Systems (TOS), Steinbachstraße 15, 52074 Aachen

Christoph Aretzweiler and Stefan Esser (Institute of Complex Systems, Cellular Biophysics, ICS-4, Forschungszentrum Jülich GmbH, 52428 Jülich, Germany) were of great practical help with IHC stainings.

Dr. Janis Brusius (Institute of Complex Systems, Cellular Biophysics, ICS-8, Forschungszentrum Jülich GmbH, 52428 Jülich, Germany) provided the Matlab script for FFT analyses.

Dr. Kira Scherer (Institute of Laboratory Animal Science, University Hospital RWTH Aachen, Aachen, Germany) was of great assistance regarding animal testing – from gaining approval by the authorities to practical everyday considerations.

This work is part of AMvdM's doctoral thesis.

References

[1] Greenberg Gail. Beyond the blindfold: my life with retinitis pigmentosa. *Clin. Dermatol.*. 2005;23:640–2;discussion 642–3.

[2] Rovner Barry W, Casten Robin J. Activity loss and depression in age-related macular degeneration. *Am. J. Geriatr. Psychiatry.* 2002;10:305–10.

[3] Weyer-Wendl H, Tamm M, Walter P. Evaluation of the German version of the caregiver reaction assessment questionnaire for informal caregivers of patients with neovascular age-related macular degeneration *Ophthalmologe.* 2015.

[4] Majji A B, Humayun M S, Weiland J D, Suzuki S, D'Anna S A, Juan E. Long-term histological and electrophysiological results of an inactive epiretinal electrode array implantation in dogs. *Invest. Ophthalmol. Vis. Sci.*. 1999;40:2073–81.

[5] Wyatt J.L., Rizzo J.F. , Grumet A., Edell D., Jensen R.J.. Development of a Silicone Retinal Implant: Epiretinal Stimulation of Retinal Ganglion Cells in the Rabbit *Invest Ophthalmol Vis Sci.* 1994;35.

[6] Rizzo Joseph F, Wyatt John, Loewenstein John, Kelly Shawn, Shire Doug. Methods and perceptual thresholds for short-term electrical stimulation of human retina with microelectrode arrays. *Invest. Ophthalmol. Vis. Sci.*. 2003;44:5355–61.

[7] Javaheri Michael, Hahn David S, Lakhanpal Rohit R, Weiland James D, Humayun Mark S. Retinal prostheses for the blind. *Ann. Acad. Med. Singapore.* 2006;35:137–44.

[8] Hartong Dyonne T., Berson Eliot L., Dryja Thaddeus P.. Retinitis pigmentosa *Lancet.* 2006;368:1795–1809.

[9] Scholz C.. Perspectives on: Materials Aspects for Retinal Prostheses *J. Bioact. Compat. Polym.*. 2007;22:539–568.

[10] Koch Christian, Mokwa Wilfried, Walter Peter, Görtz Michael. First Results of a Study on a Completely Implanted Retinal Prosthesis in Blind Humans in *IEEE Sensors*:1237–1240 2008.

[11] Waschkowski Florian, Hesse Stephan, Rieck Anne Christine, et al. Development of very large electrode arrays for epiretinal stimulation (VLARS). *Biomed. Eng. Online.* 2014;13:11.

[12] Roessler Gernot, Laube Thomas, Brockmann Claudia, et al. Implantation and explantation of a wireless epiretinal retina implant device: observations during the EPIRET3 prospective clinical trial. *Invest. Ophthalmol. Vis. Sci.*. 2009;50:3003–8.

[13] Zrenner Eberhart, Bartz-Schmidt Karl Ulrich, Benav Heval, et al. Subretinal electronic chips allow blind patients to read letters and combine them to words. *Proceedings. Biol. Sci.*. 2011;278:1489–97.

[14] Menzel-Severing J., Laube T., Brockmann C., et al. Implantation and explantation of an active epiretinal visual prosthesis: 2-year follow-up data from the EPIRET3 prospective clinical trial *Eye.* 2012;26:501–509.

[15] Ahuja A. K., Yeoh J., Dorn J. D., et al. Factors Affecting Perceptual Threshold in Argus II Retinal Prosthesis Subjects *Transl. Vis. Sci. Technol.*. 2013;2:1.

[16] Dorn Jessy D., Ahuja Ashish K., Caspi Avi, et al. The Detection of Motion by Blind Subjects With the Epiretinal 60-Electrode (Argus II) Retinal Prosthesis *JAMA Ophthalmol.*. 2013;131:183.

[17] Stingl K, Bartz-Schmidt K U, Braun A, et al. Transfer characteristics of subretinal visual implants: corneally recorded implant responses. *Doc. Ophthalmol.*. 2016;133:81–90.

[18] Devenyi Robert G, Manusow Joshua, Patino Beatrice E, Mongy Mohamed, Markowitz Michelle, Markowitz Samuel N. The Toronto experience with the Argus II retinal prosthesis: new technology, new hope for patients. *Can. J. Ophthalmol.*. 2018;53:9–13.

[19] Jones Bryan W., Marc Robert E.. Retinal remodeling during retinal degeneration *Exp. Eye Res.*. 2005;81:123–137.

[20] Mohand-Said Saddek. Selective Transplantation of Rods Delays Cone Loss in a Retinitis Pigmentosa Model *Arch. Ophthalmol.*. 2000;118:807.

[21] Cideciyan Artur V, Jacobson Samuel G, Aleman Tomas S, et al. In vivo dynamics of retinal injury and repair in the rhodopsin mutant dog model of human retinitis pigmentosa *Proc. Natl. Acad. Sci. U. S. A.*. 2005;102.

[22] May Chr. Albrecht, Lütjen-Drecoll Elke, Narfström Kristina. Morphological Changes in the Anterior Segment of the Abyssinian Cat Eye with Hereditary Rod-Cone Degeneration *Curr. Eye Res.*. 2005;30:855–862.

[23] Kondo Mineo, Sakai Takao, Komeima Keiichi, et al. Generation of a Transgenic Rabbit Model of Retinal Degeneration *Investig. Ophthalmol. Vis. Sci.*. 2009;50:1371–1377.

[24] Ross Jason W., Fernandez de Castro Juan P., Zhao Jianguo, et al. Generation of an Inbred Miniature Pig Model of Retinitis Pigmentosa *Investig. Opthalmology Vis. Sci.*. 2012;53:501.

[25] Widmark E J. Über den Einfluss des Lichtes auf die vorderen Medien des Auges *Acta Physiol.*. 1889;1:264–330.

[26] Noell W.K.. Biochemistry of the Retina :51–72Academic Press, New York 1965.

[27] Organisciak Daniel T., Winkler Barry S.. Retinal light damage: Practical and theoretical considerations *Prog. Retin. Eye Res.*. 1994;13:1–29.

[28] Van Norren Dirk, Gorgels Theo G M F. The action spectrum of photochemical damage to the retina: A review of monochromatic threshold data *Photochem. Photobiol.*. 2011;87:747–753.

[29] Ham W T, Mueller H A, Ruffolo J J, Clarke A M. Sensitivity of the retina to radiation damage as a function of wavelength. *Photochem. Photobiol.*. 1979;29:735–43.

[30] Ham W T, Mueller H A, Ruffolo J J, Guerry D, Guerry R K. Action spectrum for retinal injury from near-ultraviolet radiation in the aphakic monkey. *Am. J. Ophthalmol.*. 1982;93:299–306.

[31] Van Norren Dirk, Schellekens Peter. Blue light hazard in rat *Vision Res.*. 1990;30:1517–1520.

[32] Collier R J, Zigman S. Comparison of retinal photochemical lesions after exposure to near-UV or short-wavelength visible radiation. *Prog. Clin. Biol. Res.*. 1989;314:569–75.

[33] Gorgels T G, Norren D. Ultraviolet and green light cause different types of damage in rat retina. *Invest. Ophthalmol. Vis. Sci.*. 1995;36:851–63.

[34] Henriksson Johanna Tukler, Bergmanson J. P G, Walsh James E.. Ultraviolet radiation transmittance of the mouse eye and its individual media components *Exp. Eye Res.*. 2010;90:382–387.

[35] Hafezi Farhad, Marti Andreas, Munz Kurt, Remé Charlotte E.. Light-induced Apoptosis: Differential Timing in the Retina and Pigment Epithelium *Exp. Eye Res.*. 1997;64:963–970.

[36] Wenzel A, Reme C E, Williams T P, Hafezi F, Grimm C. The Rpe65 Leu450Met variation increases retinal resistance against light-induced degeneration by slowing rhodopsin regeneration. *J. Neurosci.*. 2001;21:53–8.

[37] Wenzel Andreas, Grimm Christian, Samardzija Marijana, Remé Charlotte E.. Molecular mechanisms of light-induced photoreceptor apoptosis and neuroprotection for retinal degeneration *Prog. Retin. Eye Res.*. 2005;24:275–306.

[38] Ebert Stefanie, Walczak Yana, Remé Charlotte, Langmann Thomas. Microglial activation and transcriptomic changes in the blue light-exposed mouse retina. *Adv. Exp. Med. Biol.*. 2012;723:619–32.

[39] Schmucker Christine, Schaeffel Frank. A paraxial schematic eye model for the growing C57BL/6 mouse *Vision Res.*. 2004;44:1857–1867.

[40] Greiling Teri M.S., Clark John I. The transparent lens and cornea in the mouse and zebra fish eye *Semin. Cell Dev. Biol.*. 2008;19:94–99.

[41] Jeon C J, Strettoi E, Masland R H. The major cell populations of the mouse retina *J Neurosci.* 1998;18:8936–8946.

[42] Rösch Sarah, Johnen Sandra, Müller Frank, Pfarrer Christiane, Walter Peter. Correlations between ERG, OCT, and Anatomical Findings in the rd10 Mouse. *J. Ophthalmol.*. 2014;2014:874751.

[43] Rösch S., Johnen S., Mataruga A., Muller F., Pfarrer C., Walter P.. Selective Photoreceptor Degeneration by Intravitreal Injection of N-Methyl-N-Nitrosourea *Invest. Ophthalmol. Vis. Sci.*. 2014;55:1711–1723.

[44] Mataruga Anja, Kremmer Elisabeth, Müller Frank. Type 3a and type 3b OFF cone bipolar cells provide for the alternative rod pathway in the mouse retina *J. Comp. Neurol.*. 2007;502:1123–1137.

[45] Haselier Christine, Biswas Sonia, Rösch Sarah, Thumann Gabriele, Müller Frank, Walter Peter. Correlations between specific patterns of spontaneous activity and stimulation efficiency in degenerated retina. *PLoS One.* 2017;12:e0190048.

[46] Collier R J, Waldron W R, Zigman S. Temporal sequence of changes to the gray squirrel retina after near-UV exposure. *Invest. Ophthalmol. Vis. Sci.*. 1989;30:631–637.

[47] Rapp L M, Smith S C. Morphologic comparisons between rhodopsin-mediated and short-wavelength classes of retinal light damage. *Invest. Ophthalmol. Vis. Sci.*. 1992;33:3367–77.

[48] Vangsted Peter. Alterations to eye structures in hairless mice by long-term ultraviolet irradiation - A histopathological study *Acta Ophthalmol.*. 1985;63:199–206.

[49] Shinomiya Katsuhiko, Ueta Mayumi, Kinoshita Shigeru. A new dry eye mouse model produced by exorbital and intraorbital lacrimal gland excision *Sci. Rep.*. 2018;8:1–10.

[50] Swan KC. Use of methyl cellulose in ophthalmology *Arch. Ophthalmol.*. 1945;33:378–380.

[51] McMillan T. J., Leatherman E., Ridley A., Shorrocks J., Tobi S. E., Whiteside J. R.. Cellular effects of long wavelength UV light (UVA) in mammalian cells *J. Pharm. Pharmacol.*. 2008;60:969–976.

[52] McCulloch Daphne L., Marmor Michael F, Brigell Mitchell G, et al. ISCEV Standard for full-field clinical electroretinography (2015 update) *Doc. Ophthalmol.*. 2015;130:1–12.

[53] Biswas Sonia, Haselier Christine, Mataruga Anja, Thumann Gabriele, Walter Peter, Müller Frank. Pharmacological Analysis of Intrinsic Neuronal Oscillations in rd10 Retina *PLoS One.* 2014;9:e99075.

[54] Goo Yong Sook, Ahn Kun No, Song Yeong Jun, et al. Spontaneous Oscillatory Rhythm in Retinal Activities of Two Retinal Degeneration (rd1 and rd10) Mice *Korean J. Physiol. Pharmacol.*. 2011;15:415–422.

[55] Jae Seol A, Ahn Kun No, Kim Ji Young, Seo Je Hoon, Kim Hyong Kyu, Goo Yong Sook. Electrophysiological and Histologic Evaluation of the Time Course of Retinal Degeneration in the rd10 Mouse Model of Retinitis Pigmentosa *Korean J. Physiol. Pharmacol.*. 2013;17:229–235.

[56] Toychiev A. H., Ivanova E., Yee C. W., Sagdullaev B. T.. Block of Gap Junctions Eliminates Aberrant Activity and Restores Light Responses during Retinal Degeneration *J. Neurosci.*. 2013;33:13972–13977.

[57] Gargini Cludia, Terzibasi Eva, Mazzoni Francesca, Strettoi Enrica. Retinal Organization in the retinal degeneration 10 (rd10) Mutant Mouse: a Morphological and ERG Study *J. Comp. Neurol.*. 2007;500:222–238.

[58] Biswas Sonia. *Immunohistochemical and electrophysiological characterization of the mouse model for Retinitis Pigmentosa , rd10.* PhD thesisRWTH Aachen University 2014.

[59] Ames Adelbert, Li Ying-Ying, Heher Eliot C, Kimble Catherine Rising. Energy metabolism of rabbit retina as related to function: high cost of Na+ transport. *J. Neurosci.*. 1992;12:840–853.

[60] Tobi Simon E., Paul Nigel, McMillan Trevor J.. Glutathione modulates the level of free radicals produced in UVA-irradiated cells *J. Photochem. Photobiol. B Biol.*. 2000;57:102–112.

[61] Čejková Jitka, Štípek S., Crkovská J., et al. UV Rays, the Prooxidant/Antioxidant Imbalance in the Cornea and Oxidative Eye Damage *Physiol. Res.*. 2004;53:1–10.

[62] Cejka Cestmir, Cejkova Jitka. Oxidative stress to the cornea, changes in corneal optical properties, and advances in treatment of corneal oxidative injuries *Oxid. Med. Cell. Longev.*. 2015;2015.

[63] Giblin Frank J., Leverenz Victor R., Padgaonkar Vanita A., et al. UVA light in vivo reaches the nucleus of the guinea pig lens and produces deleterious, oxidative effects *Exp. Eye Res.*. 2002;75:445–458.

[64] Kielbassa C, Roza L, Epe B. Wavelength dependence of oxidative DNA damage induced by UV and visible light. *Carcinogenesis.* 1997;18:811–816.

[65] Kvam E, Tyrrell R M. Induction of oxidative DNA base damage in human skin cells by UV and near visible radiation. *Carcinogenesis.* 1997;18:2379–2384.

[66] Peak M J, Peak J G, Jones C A. Different (direct and indirect) mechanisms for the induction of DNA-protein crosslinks in human cells by far- and near-ultraviolet radiations (290 and 405 nm). *Photochem. Photobiol.*. 1985;42:141–6.

[67] Yoshimura Nagahisa, Hangai Masanori. *OCT Atlas.* Springer Medizin 2014.

[68] DeVries Steven H., Baylor Denis A.. Mosaic Arrangement of Ganglion Cell Receptive Fields in Rabbit Retina *J. Neurophysiol.*. 1997;78:2048–2060.

[69] Baden Tom, Berens Philipp, Franke Katrin, Román Rosón Miroslav, Bethge Matthias, Euler Thomas. The functional diversity of retinal ganglion cells in the mouse *Nature.* 2016;529:345–50.

[70] Algvere P. V., Torstensson P. A L, Tengroth B. M.. Light transmittance of ocular media in living rabbit eyes *Investig. Ophthalmol. Vis. Sci.*. 1993;34:349–354.

[71] Walsh J E, Bergmanson J P, Koehler L V, Doughty M J, Fleming D P, Harmey J H. Fibre optic spectrophotometry for the in vitro evaluation of ultraviolet radiation (UVR) spectral transmittance of rabbit corneas *Physiol Meas.* 2008;29:375–388.

[72] Čejka Č, Plátenník J., Širc J., et al. Changes of corneal optical properties after UVB irradiation investigated spectrophotometrically *Physiol. Res.*. 2010;59:591–597.

[73] Douglas R H, Jeffery G. The spectral transmission of ocular media suggests ultraviolet sensitivity is widespread among mammals. *Proc. Biol. Sci.*. 2014;281:20132995.

[74] Tsukahara Naoki, Tani Yuri, Kikuchi Hideyuki, Sugita Shoei. Light transmission of the ocular media in birds and mammals. *J. Vet. Med. Sci.*. 2014;76:93–5.

Supplementary Material

Dosage Calculation

The corneal irradiance was calculated based on the specifications of the LED array: Illumination diameter FWHM at working distance of 100 mm = 46.5 mm; irradiance at 100 mm = 106 W/m² (≙ 0.106 mW/mm²). With the total distance of 20 mm from LED array to corneal surface in our setup, we calculated the light cone diameter at that distance (= 37.3 mm) with trigonometry. With the light cone diameter, the illuminated area at 100 mm was calculated (= 1698 mm²) and multiplied with 0.106 mW/mm², resulting in a power of 180 mW. To get the intensity at 20 mm distance, the calculated power was divided by the illuminated area at 20 mm (= 1092 mm²), resulting in 16.47 mW/cm². To get the time of irradiance for a certain dosage, the dosage (e.g., 7.5 J/cm²) was multiplied with the area at 20 mm distance of 1092 mm², resulting in an energy of 81.9 J in this example. This energy divided by the power at 20 mm distance (16.47 W) equals a time of 497 s (≙ 8 minutes and 17 seconds).

Antibodies

The antibodies used in this study as well as the dilution they were applied in and the source they wer acquired from are stated in the table below.

Table 3: Overview of used Antibodies.
α = anti; ch = chicken; d = donkey; gp = guinea pig; gt = goat; ms = mouse; rb = rabbit; rt = rat

Primary Antibody	**Dilution**	**Source**	**Secondary Antibody**	**Dilution**	**Source**
anti-protein kinase C alpha ($PKC\alpha^{rb}$)	1:4000	Santa Cruz Biotechnology Inc., Heidelberg, Germany	dαrb Cy2	1:400	Dianova GmbH, Hamburg, Germany
anti-calcium binding protein 28K ($CabP^{ms}$)	1:1000	Sigma-Aldrich Chemie GmbH, Hamburg, Germany	dαms Cy3	1:100	Dianova
anti-calretinin (Cal^{gt}) AB1550	1:3000	Millipore, Schwalbach, Germany	dαgt Alexa 647	1:200	Invitrogen AG, Carlsbad, CA, USA

continue on the next page

Table 3: Overview of used Antibodies ... (cont.)

Primary Antibody	**Dilution**	**Source**	**Secondary Antibody**	**Dilution**	**Source**
anti-recoverin (Rec^{rb}) Ab5585	1:2000	Millipore	gtαrb Alexa 488	1:500	Invitrogen
anti-HCN1 ($HCN1^{rt}$) RTQ-7C3	1:10	F. Müller, Forschungszentrum Jülich	d αrt Cy3	1:500	Dianova
anti-rhodopsin (Rho^{ms}) 1D4	1:500	R.S. Molday, British Columbia, Canada	dαms Dy649 or Cy5	1:500	Dianova
anti-glial fibrillary acid protein ($GFAP^{ch}$)	1:2000	Novus Biologicals, Cambridge, UK	dαch Cy2	1:200	Dianova

continue on the next page

Table 3: Overview of used Antibodies ... (cont.)

Primary Antibody	**Dilution**	**Source**	**Secondary Antibody**	**Dilution**	**Source**
anti-glutamine synthetase (GS^{ms})	1:2000	BD Biosciences, Franklin Lakes, USA	dαms Cy3	1:100	Dianova
lectin peanut agglutinin (PEA, biotinylated)	1:1600	Sigma-Aldrich Chemie GmbH	Streptavidin Alexa 647 (S647 for visualization of PEA)	1:200	Invitrogen
anti-CD11b ($CD11b^{rt}$)	1:2000	Abcam plc, Cambridge, UK	gtαrt Alexa 488	1:500	Invitrogen
anti-Go-alpha ($Go\alpha^{ms}$)	1:4000	Chemicon	dαms Cy3	1:100	Dianova

continue on the next page

Table 3: Overview of used Antibodies ... (cont.)

Primary Antibody	**Dilution**	**Source**	**Secondary Antibody**	**Dilution**	**Source**
anti-HCN4 ($HCN4^{rt}$) 1A4	1:100	Millipore	gtαrt Alexa 488	1:500	Invitrogen
anti-PKA RIIb (PKA^{ms})	1:4000	BD Biosciences	dαms Cy3	1:100	Dianova
anti-piccolo ($Piccolo^{gp}$)	1:500	Synaptic Systems GmbH, Göttingen, Germany)	dαgp Cy2	1:400	Dianova
anti-mGluR6 ($mGluR6^{rb}$)	1:1000	Sigma-Aldrich	dαrb Cy3	1:500	Dianova
anti-postsynaptic density protein 95 ($PSD95^{ms}$)	1:200	Sigma-Aldrich	dαms Dy649	1:500	Dianova

sd-OCT Details

Figure 11 provides more detailed views of cross-sectional sd-OCT scans taken at 2d, 5d, 1w and 12w after irradiation.

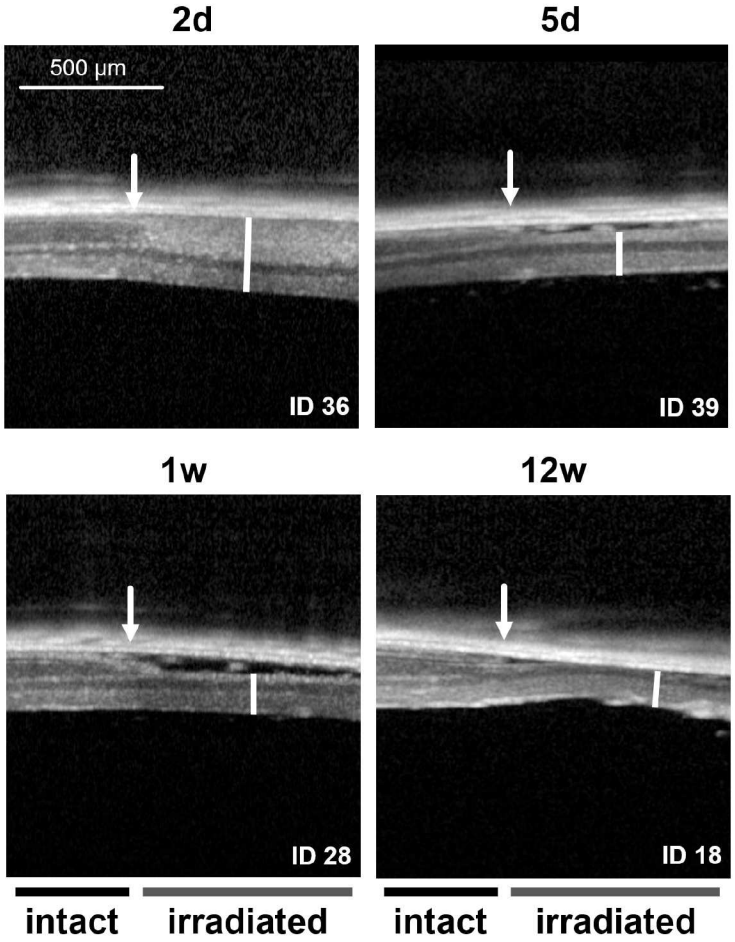

Figure 11: Detailed views of cross-sectional sd-OCT scans from treated eyes 2d, 5d, 1w and 12w after irradiation.
The intact area is displayed in the left part of the image, the irradiated area in the right part. White arrows indicate the transition from intact to irradiated areas, white bars indicate retinal thickness. Animal IDs allow assignment of scans to individual animals.

Point Estimates and p-values of OCT and ERG Statistics

Point in time	Eye	Point Estimate [µm]	SD [µm]
5d	untreated	215.6	2.2
5d	treated	161.8	2.2
1w	untreated	216.7	2.2
1w	treated	128.4	2.0
2w	untreated	214.9	2.2
2w	treated	108.9	2.0
4w	untreated	217.5	2.2
4w	treated	108.6	2.0
6w	untreated	217.5	2.2
6w	treated	104.7	2.0
8w	untreated	215.7	1.4
8w	treated	108.3	1.5
12w	untreated	215.9	2.0
12w	treated	108.0	2.0

Table 3-1: Point Estimates of sd-OCT measurements of the whole retina and Standard Deviations
SD = Standard Deviation. See Figure 5 B for the corresponding plot.

Point in time	Eye	p-value
5d	untreated vs. treated	< 0.0001
1w	untreated vs. treated	< 0.0001
2w	untreated vs. treated	< 0.0001
4w	untreated vs. treated	< 0.0001
6w	untreated vs. treated	< 0.0001
8w	untreated vs. treated	< 0.0001
12w	untreated vs. treated	< 0.0001
5d vs. 1w	treated	< 0.0001
5d vs. 2w	treated	< 0.0001
5d vs. 4w	treated	< 0.0001
5d vs. 12w	treated	< 0.0001
1w vs. 2w	treated	< 0.0001
1w vs. 4w	treated	< 0.0001
2w vs. 4w	treated	0.9970
4w vs. 6w	treated	0.6828
4w vs. 8w	treated	0.9970
4w vs. 12w	treated	0.9970

Table 3-2: Exact p-values of comparisons between measured overall retinal thickness from sd-OCT scans
p-values after Scheffe adjustment. See Figure 5 B for the corresponding plot.

Point in time	Eye	Point Estimate [µm]	SD [µm]
5d	untreated	113.0	1.4
5d	treated	112.0	1.4
1w	untreated	111.9	1.4
1w	treated	113.0	1.3
2w	untreated	110.1	1.4
2w	treated	108.0	1.3
4w	untreated	112.4	1.4
4w	treated	108.8	1.3
6w	untreated	113.5	1.4
6w	treated	102.9	1.3
8w	untreated	112.4	0.9
8w	treated	106.0	0.9
12w	untreated	112.1	1.3
12w	treated	107.3	1.3

Table 3-3: Point Estimates of sd-OCT measurements of the inner retina and Standard Deviations
SD = Standard Deviation. See Figure 6 for the corresponding plot.

Point in time	Eye	p-value
5d	untreated vs. treated	0.9819
1w	untreated vs. treated	0.9819
2w	untreated vs. treated	0.9732
4w	untreated vs. treated	0.9161
6w	untreated vs. treated	0.0038
8w	untreated vs. treated	0.0201
12w	untreated vs. treated	0.6684
5d vs. 1w	treated	0.9819
5d vs. 2w	treated	0.8664
5d vs. 4w	treated	0.9161
5d vs. 6w	treated	0.0237
5d vs. 8w	treated	0.2921
5d vs. 12w	treated	0.7037
1w vs. 2w	treated	0.5944
1w vs. 4w	treated	0.7453
2w vs. 4w	treated	0.9819
4w vs. 6w	treated	0.3896
4w vs. 8w	treated	0.9161
4w vs. 12w	treated	0.9809

Table 3-2: Exact p-values of comparisons between measured inner retinal thickness from sd-OCT scans
p-values after Scheffe adjustment. See Figure 6 for the corresponding plot.

Point in time	Eye	Point Estimate [µV] ±SD [µV]			
		B	C1	C2	D
5d	untreated	160.9 ±11.9	186.4 ±16.4	394.8 ±28.1	89.9 ±8.8
5d	treated	70.5 ±11.6	101.2 ±15.8	160.8 ±27.7	41.5 ±8.6
1w	untreated	246.2 ±11.5	304.1 ±14.8	608.3 ±27.2	111.8 ±6.9
1w	treated	87.9 ±11.4	125.0 ±14.6	218.6 ±26.8	45.0 ±6.8
2w	untreated	215.8 ±11.5	266.1 ±14.8	559.9 ±27.2	111.7 ±7.5
2w	treated	89.6 ±11.4	132.0 ±14.6	239.0 ±26.8	46.4 ±8.2
4w	untreated	215.5 ±10.7	275.1 ±14.8	530.6 ±27.2	112.3 ±6.5
4w	treated	102.0 ±10.6	142.7 ±14.6	236.9 ±26.8	54.3 ±6.8
6w	untreated	197.5 ±10.7	264.4 ±14.8	546.7 ±27.2	96.4 ±6.5
6w	treated	86.7 ±10.6	133.8 ±14.6	242.9 ±26.8	47.3 ±6.8
8w	untreated	198.1 ±7.5	254.4 ±10.4	500.9 ±19.0	102.6 ±5.0
8w	treated	131.4 ±7.5	177.6 ±10.3	300.9 ±19.2	55.9 ±5.1
12w	untreated	188.7 ±9.9	236.0 ±13.4	505.3 ±24.7	87.1 ±5.9
12w	treated	118.7 ±9.9	154.1 ±13.3	296.3 ±25.0	55.6 ±6.0

Table 4-1: Point estimates and standard deviations (SD) of a- and b-waves from ffERGs
Column B, C1, C2 and D correspond to the respective plots in Figure 7.

Point in time	Eye	p-value			
		B	C1	C2	D
5d	untreated vs. treated	0.0008	0.0121	< 0.0001	0.0281
1w	untreated vs. treated	< 0.0001	< 0.0001	< 0.0001	< 0.0001
2w	untreated vs. treated	< 0.0001	< 0.0001	< 0.0001	0.0005
4w	untreated vs. treated	< 0.0001	< 0.0001	< 0.0001	0.0002
6w	untreated vs. treated	< 0.0001	< 0.0001	< 0.0001	0.0016
8w	untreated vs. treated	0.0002	0.0005	< 0.0001	0.0001
12w	untreated vs. treated	0.0048	0.0088	< 0.0001	0.0644
5d vs. 1w	untreated	0.0048	0.0044	0.0017	0.8909
5d vs. 12w	untreated	0.3982	0.3908	0.2053	0.9988
1w vs. 2w	untreated	0.3982	0.3908	0.3650	0.9988
1w vs. 4w	untreated	0.3982	0.3908	0.2839	0.9988
1w vs. 6w	untreated	0.1271	0.3908	0.3650	0.8909
1w vs. 8w	untreated	0.1084	0.3711	0.1767	0.9504
1w vs. 12w	untreated	0.0923	0.1784	0.2053	0.5370
5d vs. 1w	treated	0.3982	0.3908	0.3650	0.9988
5d vs. 12w	treated	0.1271	0.3711	0.1102	0.9225

Table 4-2: Exact p-values of comparisons between recorded a- and b-waves from ffERGs
p-values after Scheffe adjustment. Column B, C1, C2 and D correspond to the respective plots in Figure 7.

IHC Stainings of Microglia

During the time span of PR degeneration, we observed a strong infiltration of the illuminated area by microglia (Figure 12). Their number reached a peak at 4d and 5d after irradiation. In combined CD11b and TO-PRO®3 stainings (data not shown), microglia cells appeared around "basophilic inclusions" (see also Figure 9 C).

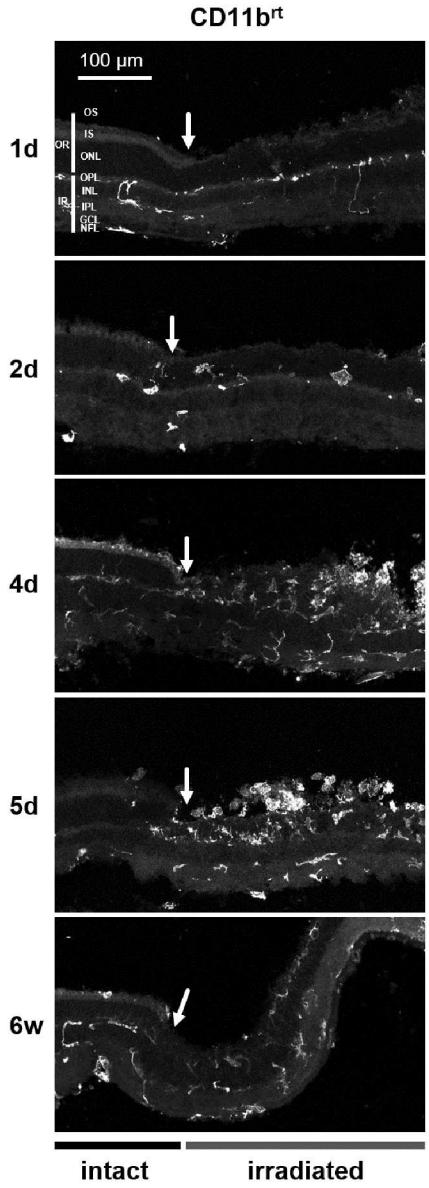

Figure 12: IHC microglia staining (S4) 1d, 2d, 4d, 5d and 6w after irradiation with 7.5 J/cm² at the transition zones between irradiated and non-irradiated retina.
All images depict parts of the retina where the transition from intact (left part of each picture) to irradiated (right part of each picture) areas of the retina is visible. Arrows indicate location of transition. All images from retinae of a treated eye in the characterization study (7.5 J/cm²). Staining: anti-CD11b (grey, microglia). Top row: 1d after irradiation; second row: 2d after irradiation; third row: 4d after irradiation, fourth row: 5d after irradiation. bottom row: 6w after irradiation.
Abbreviations as in Fig. 5.

MEA Recordings of WT, rd10 and MNU mice

In order to be able to directly compare oscillatory potentials of the UV-induced model of PR degeneration to those of the rd10 and MNU mouse, traces of 50 Hz lowpass filtered data of MEA recordings (taken from [45]) are shown in Figure 13.

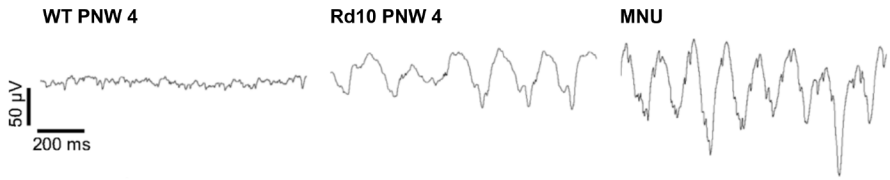

Figure 13: 50 Hz lowpass filtered data from MEA recordings, taken and adapted from [45].
Wildtype (WT) and rd10 trace recorded at postnatal week 4 (PNW 4). MNU trace recorded 11 days after treatment. [45]

MEA Recordings: Electrical and Light Stimulation

Procedure

For general procedure, please refer to Section Material and Methods - MEA Recordings. Electrical stimulation pulses with 20-100 µA and a duration of 1000 µs per phase (cathodic phase first, anodic phase second) were applied with increasing intensity. Before and in between the electrical stimulations, spontaneous activity was recorded. After that, the retina was dark adapted for 30 minutes and stimulated with a light pulse 2-3 times with at least 30 seconds recovery time in between the light pulses. As light source a hand-held LED was used, that was switched on and off manually.

Analysis

Electrical Stimulation: A bandpass filter (200 - 3000 Hz) was applied and the data were imported into Offline Sorter (3.3.2, Plexon Inc., Dallas, TX, USA),

where a spike sorting was performed based on the action potentials' slope. The spike sorted data were imported into NeuroExplorer (4.125, Nex Technologies, Madison, AL, USA) and spike frequencies 5 s before and 500 ms after stimulus application were compared in perievent histograms. Frequency ratios (= spike frequency 500 ms after stimulus divided by spike frequency 5 s before stimulus) were calculated for further evaluation. In treated eyes, data were sorted into channels that were covered with irradiated retina and channels that were covered with intact retina. Means were calculated from these categories from each animal. In untreated eyes, a categorization was not necessary. Electrical stimulation intensities were categorized into three subsets, according to the amplitude of the stimulation current. Comparisons within one subset (same stimulation current, comparison between degenerated and intact retina of one treated eye) were performed with paired t-tests, comparisons between subsets (untreated eyes and degenerated or intact areas of treated eyes remained constant; comparison between stimulation currents) were performed with paired t-tests and comparisons between untreated and treated (irradiated or intact area) eyes were compared via unpaired t-tests. The data of treated eyes from mice whose untreated eyes were used for analysis, were excluded from the analysis of treated data sets, in order to perform unpaired t-tests.

Light Stimulation: For light stimulation analysis, the same procedure as for electrical stimulation was used. Spike frequencies were compared 10 seconds before, and 1 second after the stimulus and evaluated in NeuroExplorer. Again, frequencies of single channels of one animal were summarized as a mean value, after categorization into electrodes covered with irradiated/degenerated and electrodes covered with intact retina. Paired t-tests were performed with data from irradiated vs. intact areas, unpaired t-tests were performed with treated vs. untreated eyes.

Results

We recently reported that stimulation efficiency was lower in degenerated retina than in WT retina [45]. We expected that intact areas of retinae from treated eyes would respond to electrical stimulation similar to retinae from untreated eyes and that irradiated areas would be more difficult to stimulate (compare [45]). We grouped our experiments according to the amplitude of stimulation currents (3-5 µA, 6-17 µA, 20-35 µA). The responses to 3-5 µA were generally lower than to higher currents, although the difference was highest in retinae from untreated eyes (Figure 14). However, note that in some cases data of only two animals could be included. Highest stimulation responses were achieved with 20-35 µA in untreated eyes compared with lower stimulation currents (mean frequency ratio: 6.9 at 3-5 µA, 18.0 at 6-17 µA, 22.4 at 20-35 µA). Significant differences in the frequency ratios after stimulation with 30-35 µA were found between untreated eyes vs. irradiated areas of treated eyes ($p \leq 0.001$) and untreated eyes vs. intact areas of treated eyes ($p \leq 0.05$).

In summary, the responses of untreated eyes were generally higher than those of treated eyes – irradiated or intact – although intact areas of treated eyes had the tendency to a higher frequency ratio than irradiated areas of treated eyes.

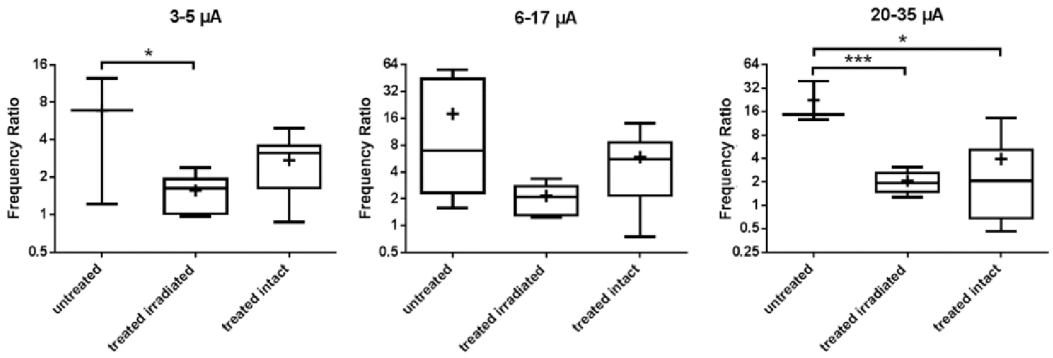

Figure 14: Analysis of the electrical stimulation of irradiated retinae ($7.5\,J/m^2$).
Comparison of stimulation with 3-5 µA, 6-17 µA and 20-35 µA (rectangular pulses, cathodic phase first, 1000 µs per phase). Cumulated data from all groups are plotted. Frequency ratio = (spike frequency 500 ms after stimulus)/(spike frequency 5 s before stimulus). Data from treated eyes of animals whose untreated eyes were used as controls, were excluded from treated data sets for unpaired t-test analysis. y-axis log2; + = mean; *** $p \leq 0.001$; * $p \leq 0.05$; untreated: 3-5 µA n = 2, 6-17 µA n = 4, 20-35 µA n = 2; irradiated areas of treated eyes: 3-5 µA n = 9, 6-17 µA n = 10, 20-35 µA n = 11; intact areas of treated eyes: 3-5 µA n = 7, 6-17 µA n = 7, 20-35 µA n = 7. paired t-test: treated eye irradiated area vs. treated eye intact area; unpaired t-test: untreated eye vs. treated eye. Only comparisons with significant differences are displayed. All other comparisons were not significant.

In light stimulation experiments there was a tendency for intact areas of treated eyes to respond better to light stimulation than irradiated areas of treated eyes. As in the electrical stimulation experiments, the intact area of treated eyes did not respond as strongly as untreated eyes. Even in irradiated areas of treated eyes, sometimes strong bursts of action potentials were found that correlated with the light stimulus (data not shown). They might reflect spontaneously occurring bursts that coincided with the light stimulus. Alternatively, as the irradiated area was close to the optic nerve head, light responses observed in this area might have been recorded from pervading axons of ganglion cells residing in the untreated area.